ARGONNE NATIONAL LABORATORY
9700 South Cass Avenue, Argonne, Illinois 60439

ANL-92/21

Dynamic Stability of Maglev Systems

by

Y. Cai, S. S. Chen, and T. M. Mulcahy

Materials and Components Technology Division

D. M. Rote

Center for Transportation Research

April 1992

MASTER

Contents

Figures

Table

Dynamic Stability of Maglev Systems

by

Y. Cai, S. S. Chen, T. M. Mulcahy, and D. M. Rote

Abstract

Because dynamic instability is not acceptable for any commercial maglev systems, it is important to consider this phenomenon in the development of all maglev systems. This study considers the stability of maglev systems based on experimental data, scoping calculations, and simple mathematical models. Divergence and flutter are obtained for coupled vibration of a three-degree-of-freedom maglev vehicle on a guideway consisting of double L-shaped aluminum segments attached to a rotating wheel. The theory and analysis developed in this study identifies basic stability characteristics and future research needs of maglev systems.

1 Introduction

The dynamic response of maglev systems is important in several respects: safety and ride quality, guideway design, and system costs. Ride quality is determined by vehicle response and by environmental factors such as humidity and noise. The dynamic response of vehicles is the key element in the determination of ride quality, and vehicle stability is one of the important elements relative to safety. To design a proper guideway that provides acceptable ride quality in the stable region, the vehicle dynamics must be understood. Furthermore, the trade-off between guideway smoothness and the levitation and control systems must be considered if maglev systems are to be economically feasible. The link between the guideway and other maglev components is vehicle dynamics. For a commercial maglev system, vehicle dynamics must be analyzed and tested in detail.

For safety, maglev systems should be stable. Magnetic forces are basically position-dependent, although some are also velocity-dependent. These motion-dependent magnetic forces can induce various types of instability. In addition, the periodic structure of the motion-dependent magnetic forces may in some cases also induce parametric and combination resonances.

Some analytical and experimental studies have been performed to understand the stability characteristics of maglev systems. Several examples are summarized briefly as follows:

1.1 Theoretic_l Studies

- Davis and Wilkie (1971) studied a magnetic coil moving over a conducting track and concluded that negative damping occurs at velocities greater than the characteristic velocity based on thin-track theory.

- Ohno et al. (1973) studied the pulsating lift forces in a linear synchronous motor. These forces may cause parametric and combination resonances, as well as heave and pitch oscillations.

- Baiko et al. (cited in Chu and Moon 1983) considered the interactions of induced eddy currents with on-board superconducting magnets and found possible heave instabilities.

1.2 Experimental Studies

- An experimental vehicle floating above a large rotating wheel was found by Moon (1974) to have sway-yaw instabilities.

- Experiments performed at MIT on a test track showed pitch-heave instability (Moon 1975).

1.3 Experimental/Analytical Studies

- A conducting guideway, consisting of L-shaped aluminum segments attached to a rotating wheel to simulate the Japanese full-scale guideway at Miyazaki, was studied experimentally and analytically by Chu and Moon (1983). Divergence and flutter were obtained for coupled yaw-lateral vibration; the divergence leads to two stable equilibrium yaw positions, and the flutter instability leads to a limit cycle of coupled yaw and lateral motions in the neighborhood of the drag peak.

- Variation of the magnetic lift force due to variation of the levitated height corresponding to the sinusoidal guideway roughness was studied by Yabuno et al. (1989). Parametric resonance of heaving and pitching motions is possible.

Based on these published analytical results and experimental data, it is obvious that different types of dynamic instabilities can occur in maglev systems. Because dynamic instability is not acceptable for any commercial maglev systems, it is important to consider this phenomenon in the development of all maglev systems.

This study considers the stability of maglev systems and is based on experimental data, scoping calculations, and simple mathematical models. The objective is to provide some basic stability characteristics and to identify future research needs.

2 Motion-Dependent Magnetic Forces

2.1 Motion-Dependent Magnetic-Force Coefficients

Magnetic forces are needed for any vehicle dynamics analysis, guideway structural design, fastening design, and prediction of ride quality. These force components are considered from the standpoint of vehicle stability.

As an example, consider a vehicle with six degrees of freedom, three translations, u_x, u_y, u_z, and three rotations, ω_x, ω_y, ω_z, as shown in Fig. 1. Let U be the vector consisting of the six motion components, i.e.,

$$U = \begin{Bmatrix} u_1 \\ u_2 \\ u_3 \\ u_4 \\ u_5 \\ u_6 \end{Bmatrix} = \begin{Bmatrix} u_x \\ u_y \\ u_z \\ \omega_x \\ \omega_y \\ \omega_z \end{Bmatrix}. \tag{1}$$

Velocity and acceleration are given by

$$\dot{U} = \frac{\partial U}{\partial t},$$

and $\hspace{10cm}$ (2)

$$\ddot{U} = \frac{\partial^2 U}{\partial t^2}.$$

The motion-dependent magnetic forces can be written
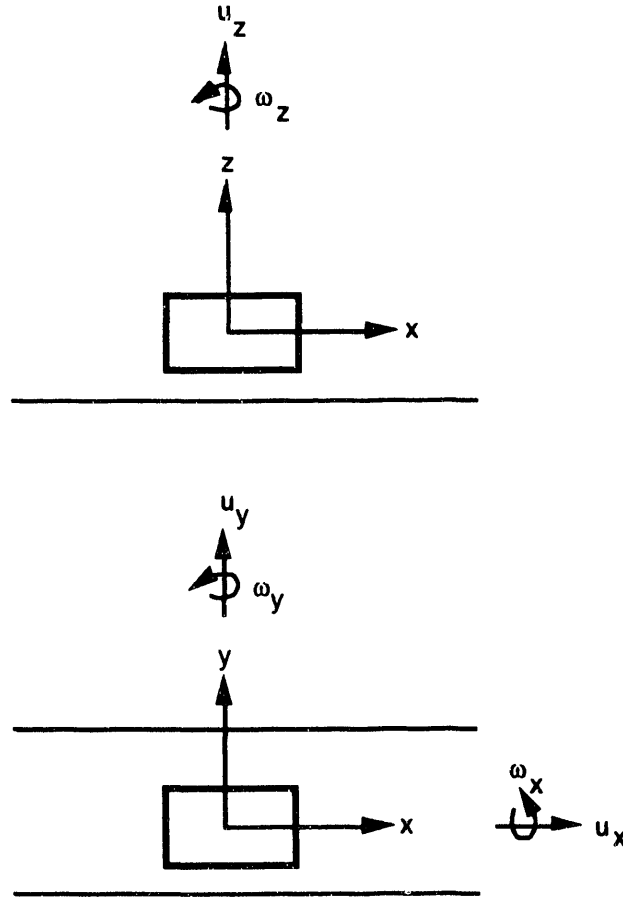
Fig. 1. Displacement components of a maglev system

$$f_i = \sum_{j=1}^{6}\left(m_{ij}\ddot{u}_j + c_{ij}\dot{u}_j + k_{ij}u_j\right), \tag{3}$$

where m_{ij}, c_{ij}, and k_{ij} are magnetic mass, damping, and stiffness coefficients. These coefficients can be obtained analytically, numerically, or experimentally and are functions of the system parameters.

- Analytical Studies: Analyses for simple cases can be performed to determine the characteristics of the coefficients. For example, an analytical method may be used to identify the coefficients that can be neglected under specific conditions.

- Numerical Methods: For the general case with complicated geometries, analytical methods may not be appropriate and numerical methods will be more useful. Numerical methods (finite-

element method and boundary-element method) can be used to calculate the values of all coefficients under specific conditions.

- Experimental Techniques: Measurements of magnetic forces will give the information required to calculate magnetic-force coefficients.

2.2 Experimental Methods to Measure Motion-Dependent Magnetic-Force Coefficients

Quasistatic Motion Theory. The magnetic forces acting on an oscillating vehicle are equal, at any instant in time, to those of the same vehicle moving with a constant velocity and with specific clearances equal to the actual instantaneous values. The magnetic forces depend on the deviation from a reference state of speed and clearance, i.e., the motion-dependent magnetic forces depend only on u_j, but not $\dot{u}_j$ and $\ddot{u}_j$, so that

$$f_i = \sum_{j=1}^{6} k_{ij} u_j. \tag{4}$$

In this case, the magnetic forces are determined uniquely by vehicle position. All elements of magnetic stiffness k_{ij} can be obtained. To determine k_{ij}, the magnetic-force component f_i is measured as a function of u_j. Stiffness is given by

$$k_{ij} = \frac{\partial f_i}{\partial u_j}. \tag{5}$$

In general, k_{ij} is a function of U.

Unsteady-Motion Theory. The magnetic forces acting on an oscillating vehicle will depend on U, $\dot{U}$, and $\ddot{U}$. The magnetic force based on the unsteady-motion theory can be obtained by measuring the magnetic force acting on the vehicle oscillating in the magnetic field. For example, if the displacement component u_j is excited, its displacement is given by

$$u_j = \bar{u}_j \exp\left(\sqrt{-1}\,\omega t\right). \tag{6}$$

The motion-dependent magnetic force of the component f_i acting on the vehicle is given by

$$f_i = \left[a_{ij}\cos\left(\psi_{ij}\right) + \sqrt{-1}\, a_{ij}\sin\left(\psi_{ij}\right)\right]\bar{u}_j \exp\left(\sqrt{-1}\,\omega t\right), \tag{7}$$

where a_{ij} is the magnetic force amplitude and ψ_{ij} is the phase angle between the magnetic force and the vehicle displacement u_j. These values are measured experimentally.

Using Eqs. 3 and 6, we can also write the motion-dependent magnetic force component as

$$f_i = \left(-m_{ij}\omega^2 + \sqrt{-1}\,\omega\, c_{ij} + k_{ij}\right)\bar{u}_j \exp\left(\sqrt{-1}\,\omega t\right). \tag{8}$$

A comparison of Eqs. 7 and 8 yields

$$c_{ij} = a_{ij}\sin\left(\psi_{ij}\right)/\omega,$$

$$\tag{9}$$

$$m_{ij} = \left[k_{ij} - a_{ij}\cos\left(\psi_{ij}\right)\right]/\omega^2.$$

Based on Eqs. 5 and 9, all motion-dependent magnetic-force matrices can be determined from two experiments: quasistatic motion and unsteady motion.

If m_{ij} and c_{ij} are of no concern, the experiment using quasisteady motion is sufficient to determine k_{ij}.

2.3 Quasistatic Motion-Dependent Magnetic-Force Coefficients of Maglev System with L-Shaped Guideway

An experiment was conducted recently at Argonne National Laboratory to investigate the lift, drag, and guidance magnetic forces on an NdFeB permanent magnet moving over an aluminum (6061-T6) L-shaped ring mounted on the top surface of a 1.2-m diameter rotating wheel (shown in Fig. 2). For a given rotating speed of the wheel, the lift and guidance magnetic forces were measured as the guidance gap Y* and lift height h were varied. A schematic diagram of the measurement approach is shown in Fig. 3. Figure 4 shows those measured forces as a function of h, with Y* fixed (Y* = 5 mm and 12.7 mm), or as a function of Y* with h fixed (h = 7 mm and 12.7 mm) when the surface velocity of the lateral leg of the guideway is 36.1 m/s, the highest velocity tested.

During testing, the long side of the 25.4 x 50.8 x 6.35 mm rectangular magnet was oriented parallel to the direction of motion of the L-shaped guideway and was
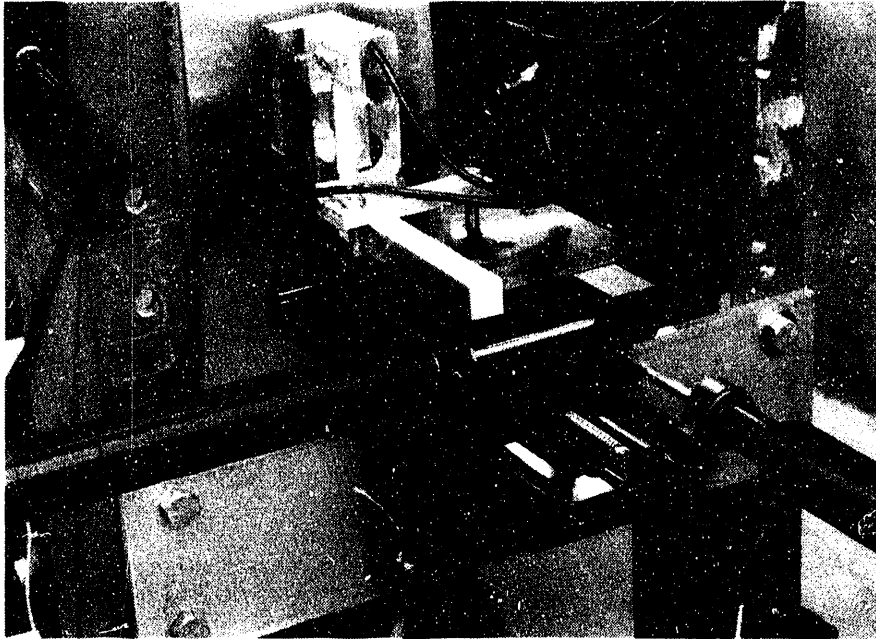
Fig. 2. Experimental apparatus for magnetic force measurement
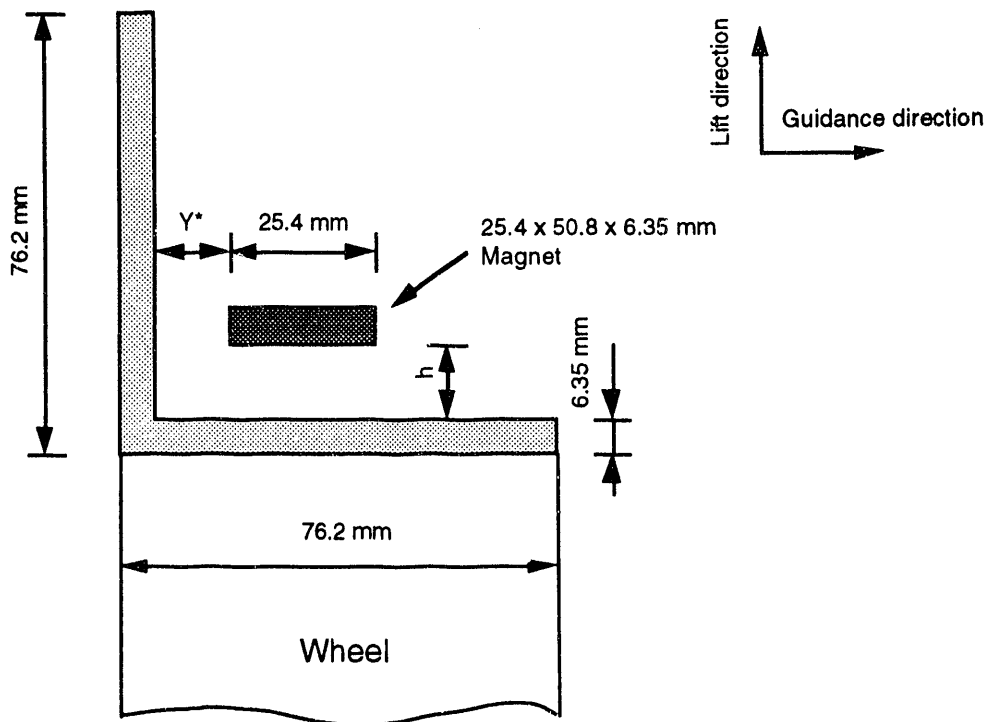
Fig. 3. Schematic diagram of the apparatus used to measure magnetic forces on an L-shaped aluminum sheet guideway

Y* = 5 mm

Y = M0 + M1*x + ... M8*x^8 + M9*x^9	
M0	2485.2072086
M1	-370.73754751
M2	25.591416346
M3	-0.93776713995
M4	0.017442074721
M5	-0.00012885295531
R	0.99997403029

(a)

Y* = 12.7 mm

Y = M0 + M1*x + ... M8*x^8 + M9*x^9	
M0	2623.4089363
M1	-410.50344932
M2	30.527419731
M3	-1.2807254486
M4	0.030650187351
M5	-0.00038829515856
M6	2.0139656841e-06
R	0.99998792531

(b)
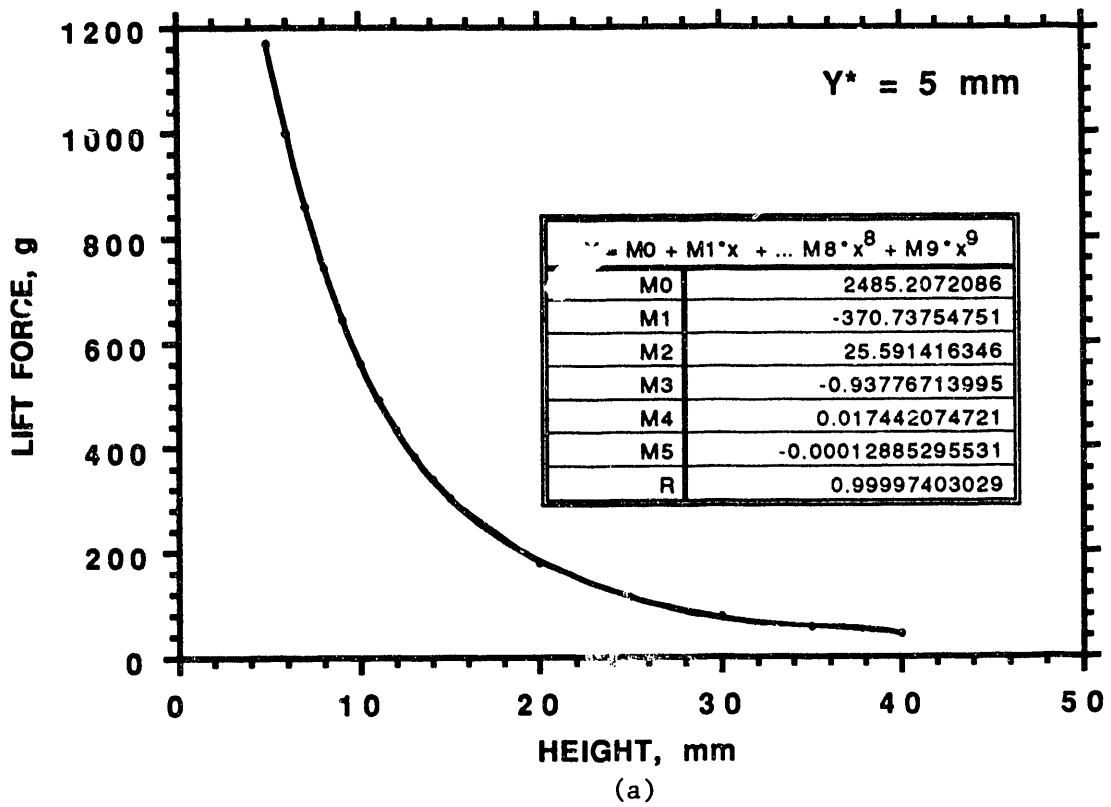
Fig. 4. Measured lift and guidance magnetic forces

Fig. 4. Cont'd

Y* = 12.7 mm

GUIDANCE FORCE, g

Y = M0 + M1*x + ... M8*x^8 + M9*x^9	
M0	25.974283328
M1	16.871081909
M2	-1.2259988206
M3	0.045480108193
M4	-0.00099175122256
M5	1.1891440675e-05
M6	-5.9728308401e-08
R	0.99990427993

HEIGHT, mm

(e)

Y* = 5 mm
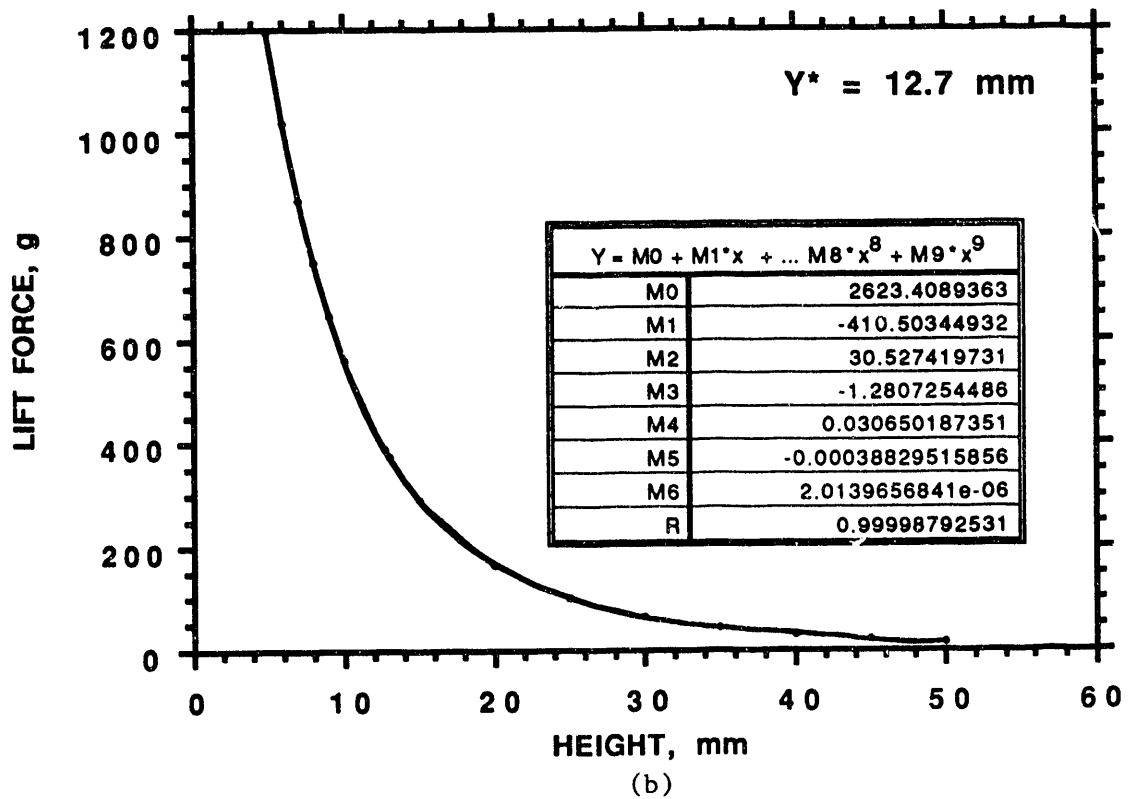
GUIDANCE FORCE, g

Y = M0 + M1*x + ... M8*x^8 + M9*x^9	
M0	271.59560866
M1	22.783510041
M2	-2.1892659951
M3	0.10217075249
M4	-0.0027202422056
M5	3.9573890684e-05
M6	-2.4621859254e-07
R	0.99991037086

HEIGHT, mm

(f)

Fig. 4. Cont'd

Y = M0 + M1*x + ... M8*x^8 + M9*x^9	
M0	860.15112485
M1	-152.23160152
M2	13.108312509
M3	-0.65046126263
M4	0.019172964592
M5	-0.00032045122602
M6	2.74293078230-06
M7	-9.15425725300-09
R	0.99997961735

h = 12.7 mm

GAP, mm

(g)

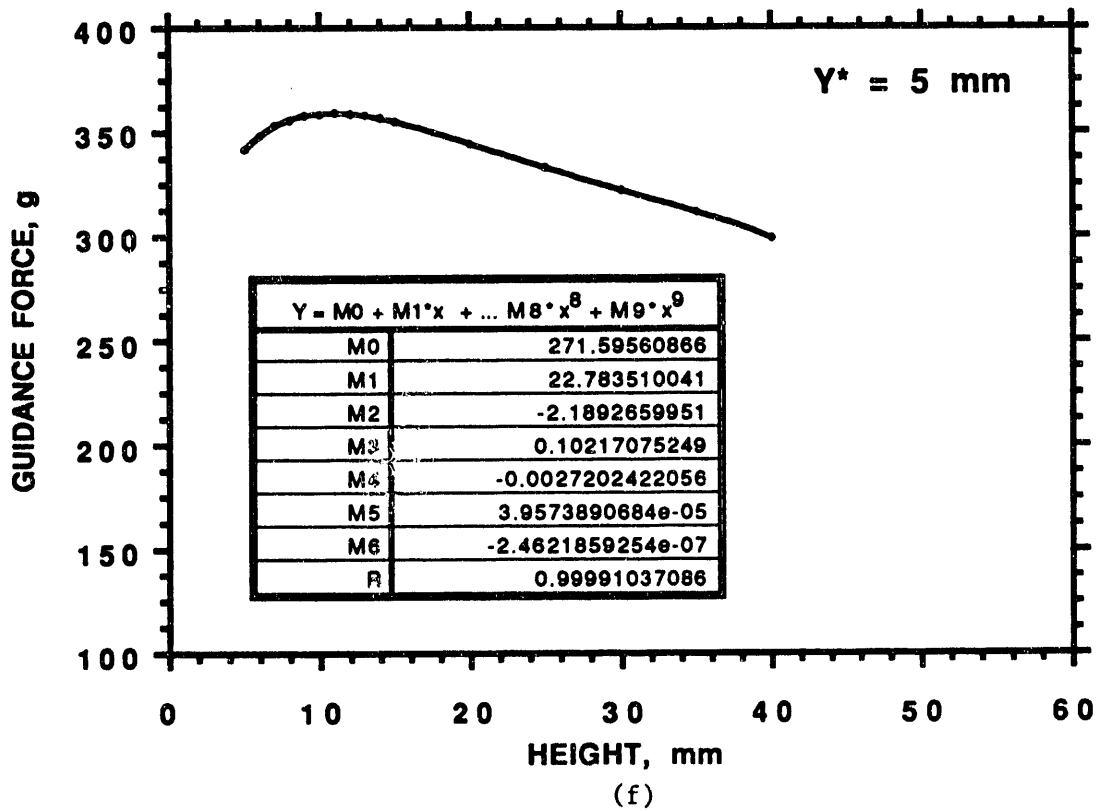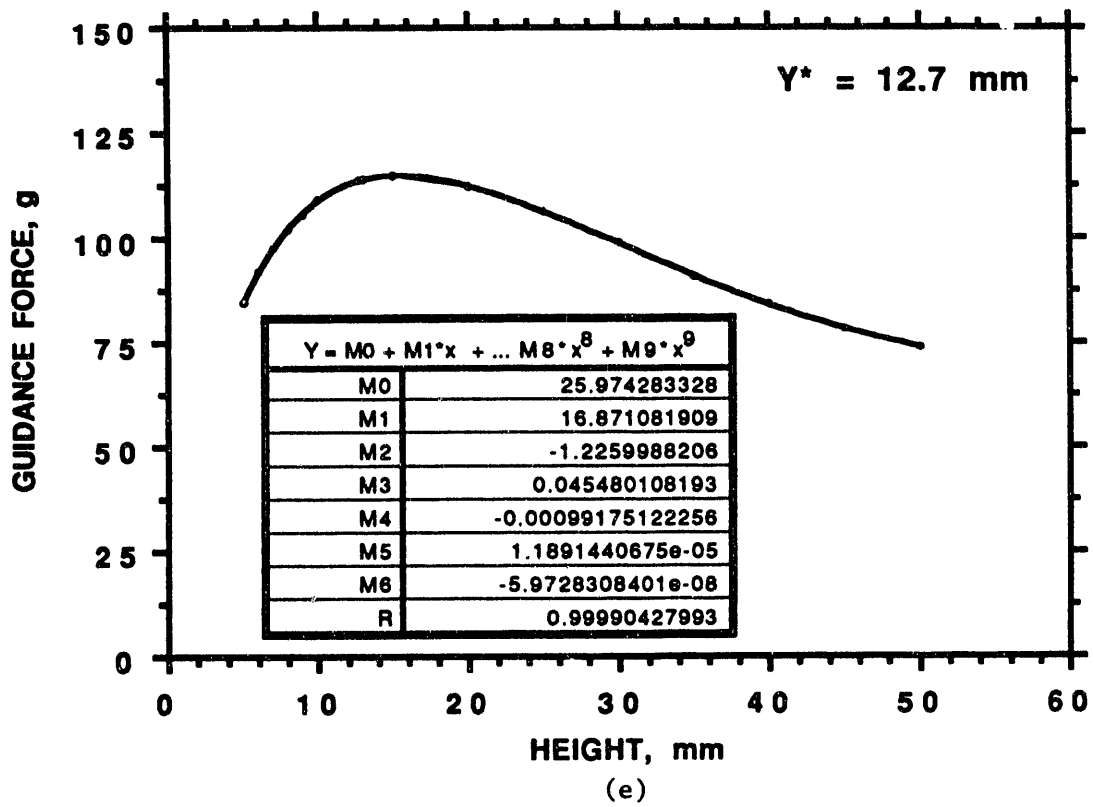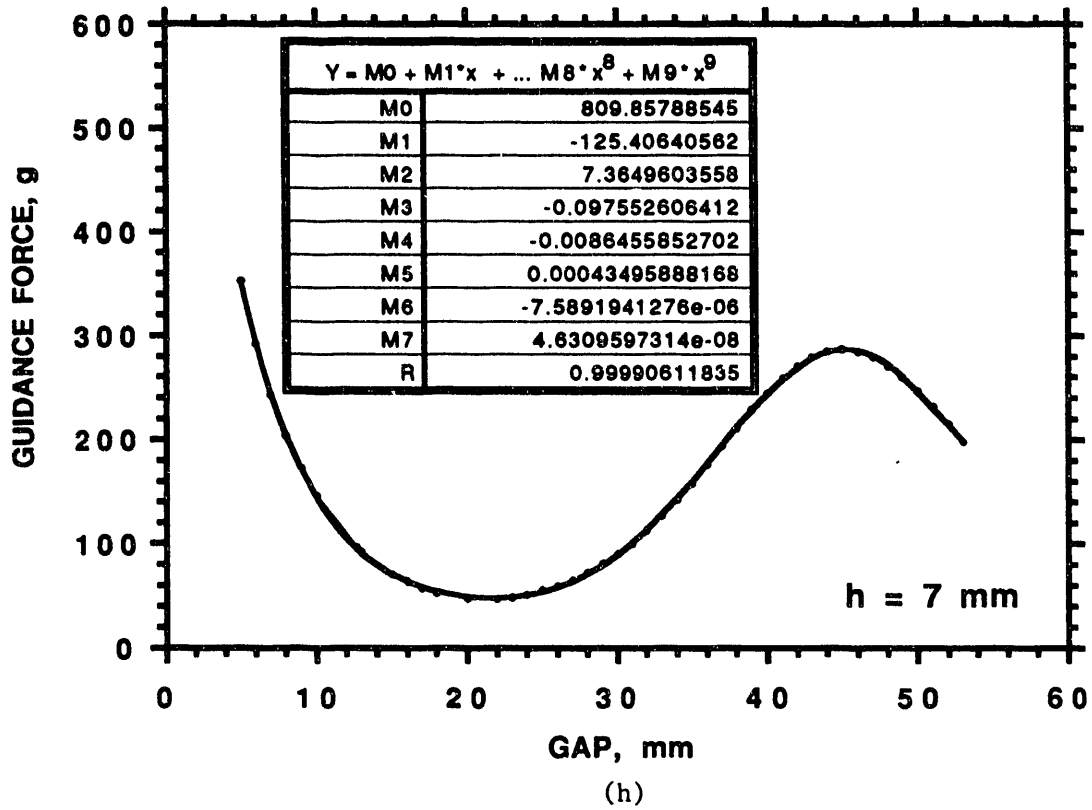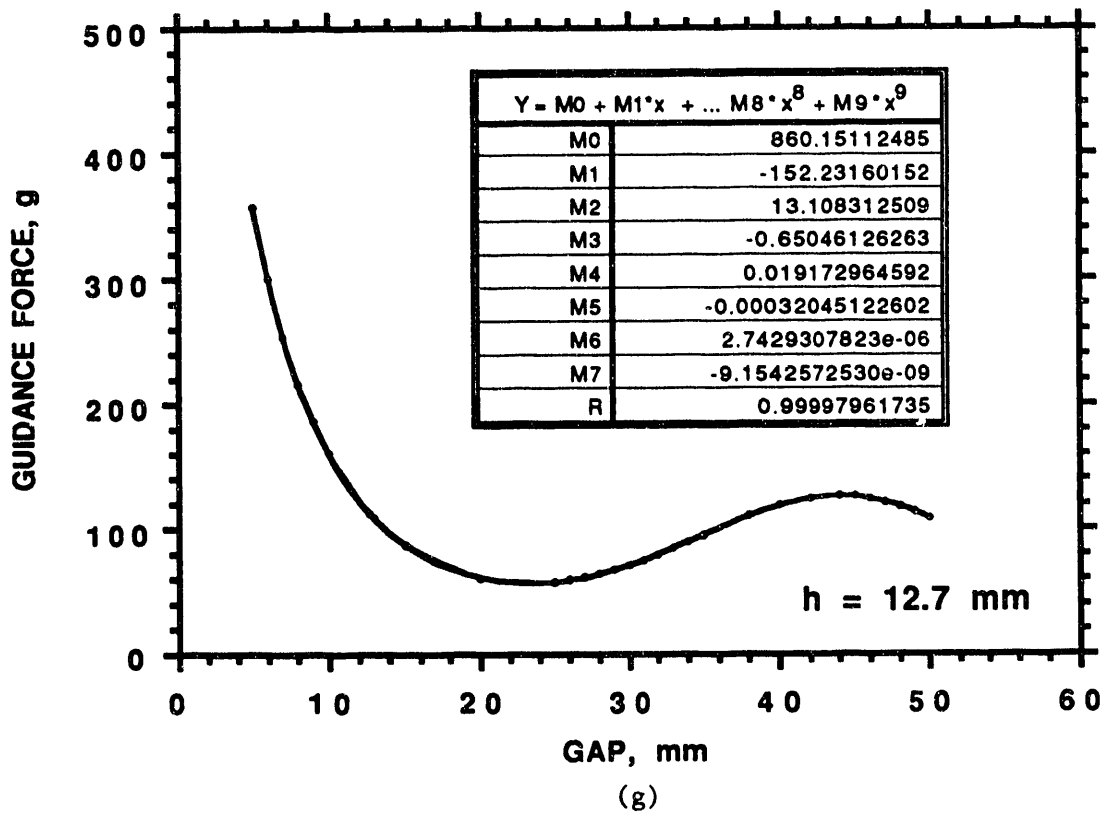| Y = M0 + M1*x + ... M8*x^8 + M9*x^9	
M0	809.85788545
M1	-125.40640562
M2	7.3649603558
M3	-0.097552606412
M4	-0.0086455852702
M5	0.00043495888168
M6	-7.58919412760-06
M7	4.63095973140-08
R	0.99990611835

h = 7 mm

GAP, mm

(h)

Fig. 4. Cont'd

held stationary by a two-component force transducer that comprised two BLH C2G1 load cells connected in series to measure the lift and guidance forces simultaneously. Laboratory weights were used to calibrate the transducer and to assess crosstalk (which was found to be <2%). The base of the load cell assembly was mounted on motorized stages that provided accurate positioning (±0.05 mm). Out-of-roundness of the L-shaped guideway ring varied, but was always less than ±0.15 mm for the lateral leg and ±0.35 mm for the vertical leg. Ability to exactly position the magnet with respect to the guideway dominated our experimental error, estimated at ±5%.

The qualitative trends in the lift and guidance force data taken at lower velocities for the L-shaped guideway are the same as shown in Fig. 4 for the highest velocity tested. Two interesting features are evident. First, a maximum occurs in the guidance force variation with respect to height variations at a fixed gap (as shown in Figs. 4e and 4f) that is caused by the corner region of the guideway. Second, a minimum occurs in the guidance force variation with respect to gap variations at a fixed height (as shown in Figs. 4g and 4h) that is caused by the edge of the lateral leg of the guideway. As will be shown in Section 4.4, the first feature is associated with a flutter and the second with a divergence instability.

Based on the magnetic force data shown in Fig. 4, we can calculate the quasistatic motion-dependent magnetic-force coefficients with Eq. 5. All elements of magnetic stiffness $k_{\ell\ell}$, $k_{\ell g}$, $k_{g\ell}$, and k_{gg}, were calculated and are shown in Fig. 5 with various Y* and h.

The curve fits to both magnetic forces and stiffnesses were derived with polynomial expressions (results are given in Figs. 4 and 5) and input into a computer code to simulate coupled vibrations of the maglev vehicle.
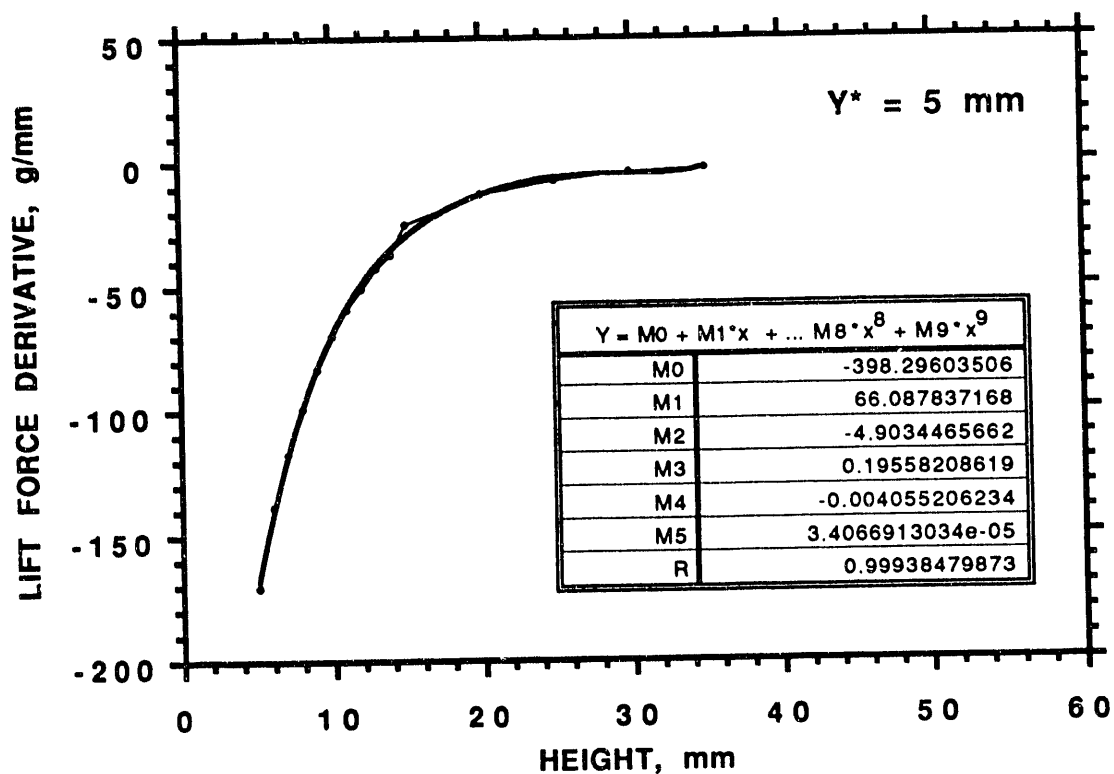
3 Stability of Maglev Systems

Without motion-dependent magnetic forces, the equation of motion for the vehicle can be written as

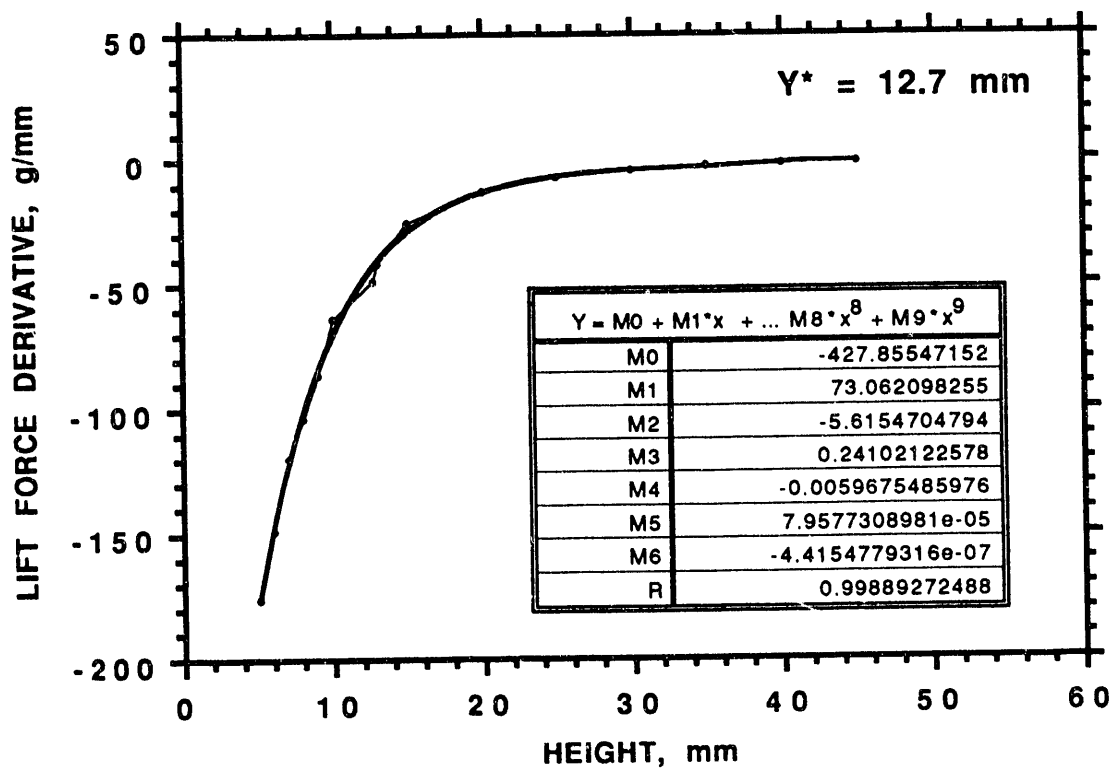$$[M_v]\{\ddot{U}\} + [C_v]\{\dot{U}\} + [K_v]\{U\} = \{Q\}, \tag{10}$$

where M_v is the vehicle mass matrix, C_v is the vehicle damping matrix, K_v is the vehicle stiffness matrix, and Q is the generalized excitation force.

The motion-dependent magnetic forces are given in Eq. 3. With motion-dependent magnetic forces, Eq. 10 becomes

Fig. 5. Measured lift and guidance magnetic stiffness

Fig. 5. Cont'd

Y* = 5 mm

Y = M0 + M1*x + ... M8*x^8 + M9*x^9	
M0	22.407288918
M1	-4.6465429478
M2	0.35828966062
M3	-0.014296989209
M4	0.00029563595274
M5	-2.5101972190e-06
R	0.98855894203

(e)

Y* = 12.7 mm

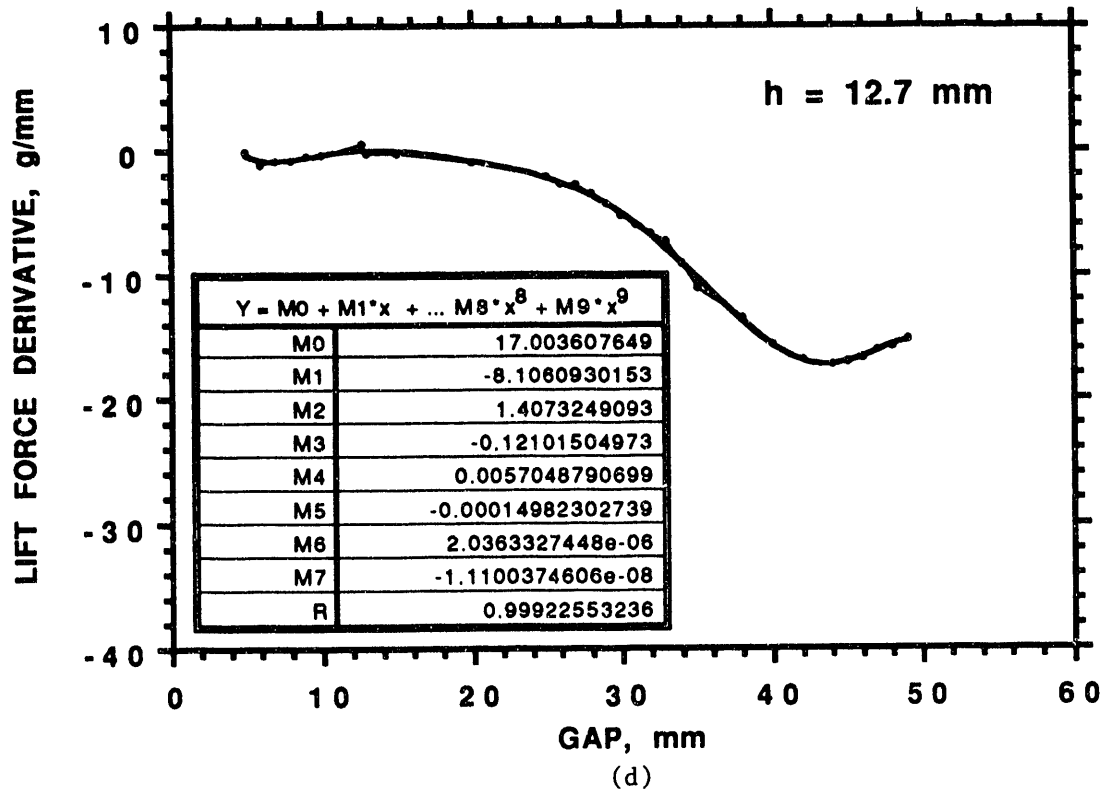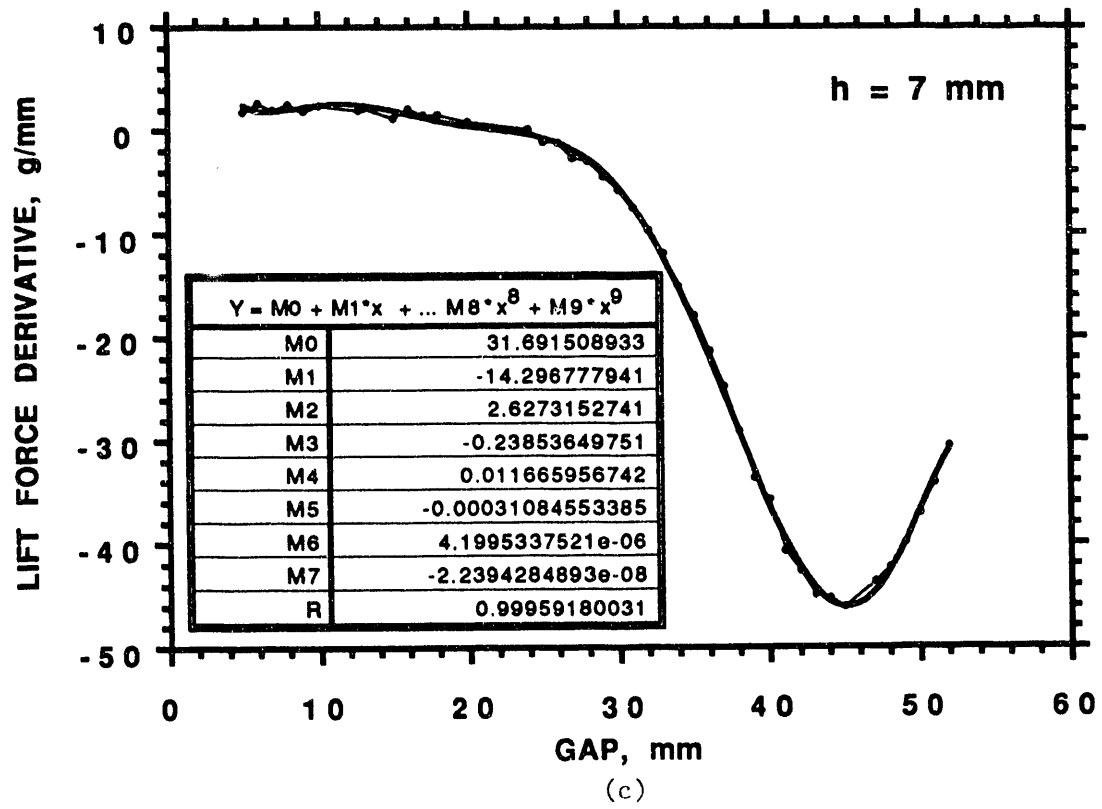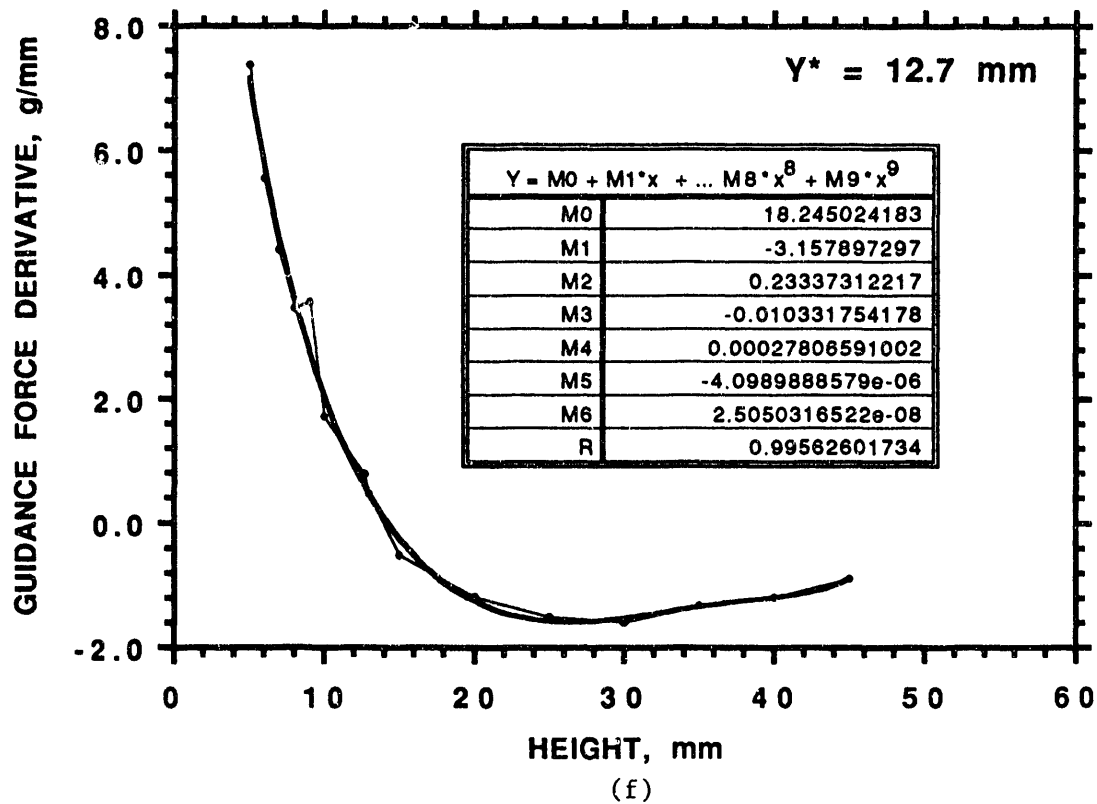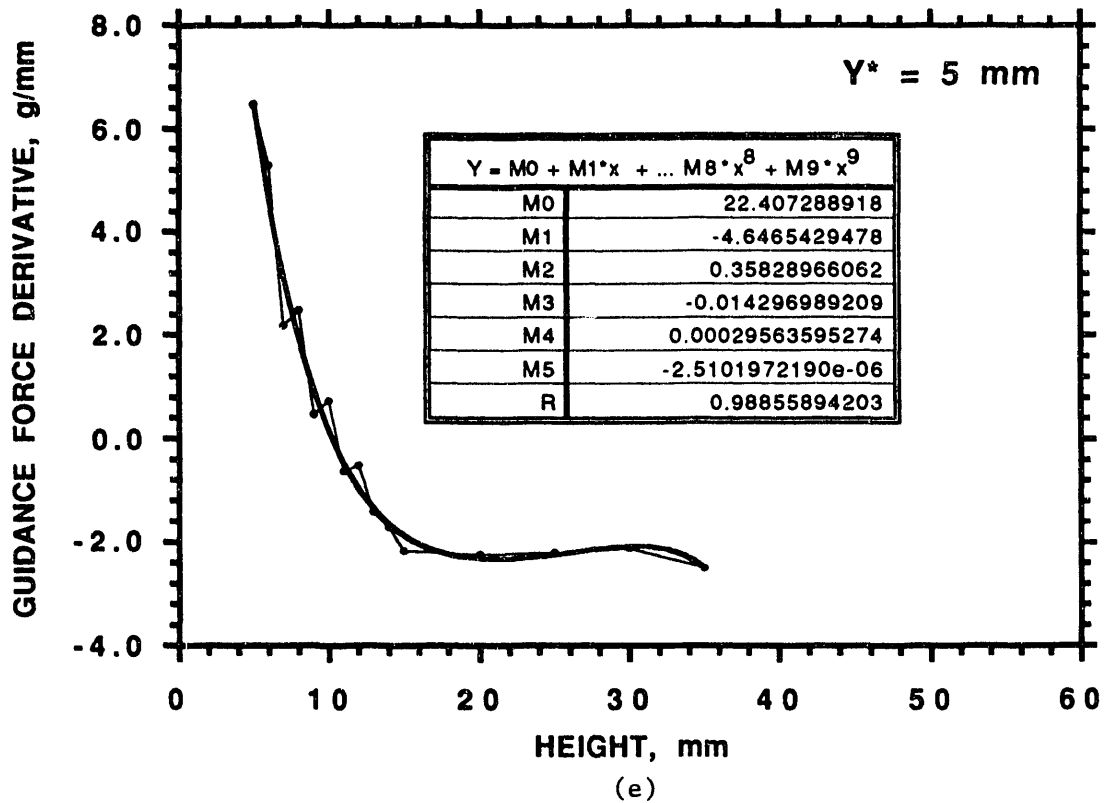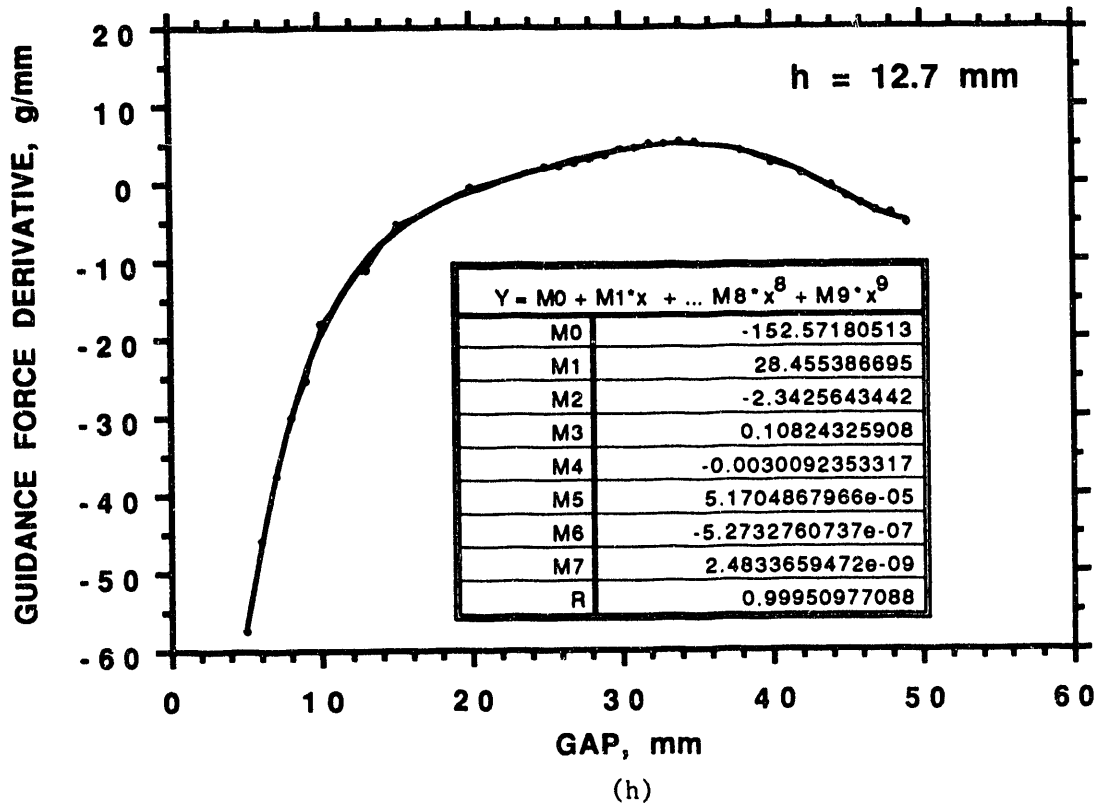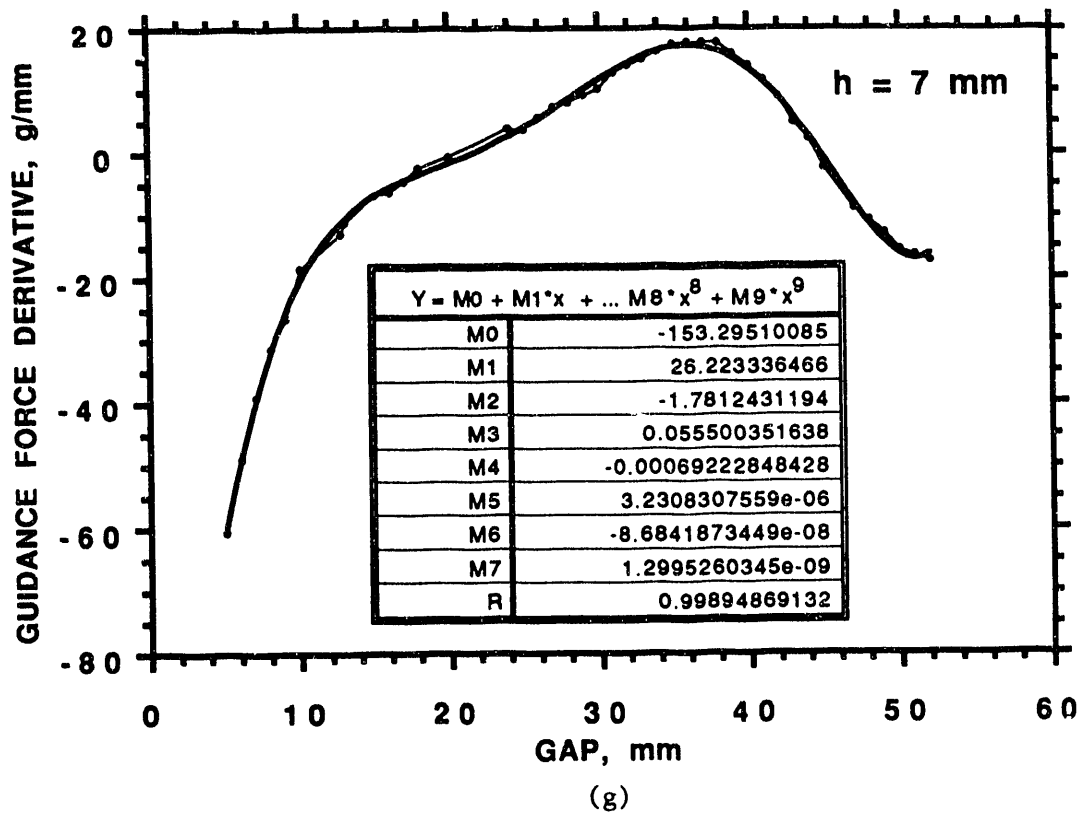| Y = M0 + M1*x + ... M8*x^8 + M9*x^9	
M0	18.245024183
M1	-3.157897297
M2	0.23337312217
M3	-0.010331754178
M4	0.00027806591002
M5	-4.0989888579e-06
M6	2.5050316522e-08
R	0.99562601734

(f)

Fig. 5. Cont'd

Fig. 5. Cont'd

$$[M_v + M_m]\{\ddot{U}\} + [C_v + C_m]\{\dot{U}\} + [K_v + K_m]\{U\} = \{Q\},$$ (11)

where M_m is the magnetic mass matrix, C_m is the magnetic damping matrix, and K_m is magnetic stiffness; their elements are m_{ij}, c_{ij}, and k_{ij}.

Once the magnetic-force coefficients are known, analysis of vehicle stability is straightforward. Equation 11 may be written as

$$[M]\{\ddot{U}\} + [C]\{\dot{U}\} + [K]\{U\} = \{Q\}.$$ (12)

In general, M, C, and K are functions of U, $\dot{U}$, and $\ddot{U}$; therefore, a complete solution is rather difficult to obtain. In many practical situations, one can ignore all nonlinear terms, so that M, C, and K are independent of vehicle motion.

By premultiplying by $\{\dot{U}\}^T$ and forming the symmetric and antisymmetric components of the matrices

$$[M_1] = \frac{1}{2}([M] + [M]^T), \qquad [M_2] = \frac{1}{2}([M] - [M]^T),$$

$$[C_1] = \frac{1}{2}([C] + [C]^T), \qquad [C_2] = \frac{1}{2}([C] - [C]^T),$$ (13)

$$[K_1] = \frac{1}{2}([K] + [K]^T), \qquad [K_2] = \frac{1}{2}([K] - [K]^T),$$

the terms may be separated, giving

$$\{\dot{U}\}^T[M_1]\{\ddot{U}\} + \{\dot{U}\}^T[C_2]\{\dot{U}\} + \{\dot{U}\}^T[K_1]\{U\}$$

$$= -\left(\{\dot{U}\}^T[M_2]\{\ddot{U}\} + \{\dot{U}\}^T[C_1]\{\dot{U}\} + \{\dot{U}\}^T[K_2]\{U\}\right).$$ (14)

Equation 14 equates rates of work. The terms on the right-hand side of the equation produce a net work-resultant when integrated over a closed path through the space {U}, the magnitude depending on the path taken. The forces corresponding to the matrices M_2, C_1, and K_2, appearing on the right-hand side, are thus, by definition, the nonconservative parts of the forces represented by M, C, and K. The terms on the left-hand side similarly can be shown to give rise to a zero work-resultant over any closed path, and therefore together are the sum of the rates of work from the potential forces and the rate of change of kinetic energy.

Different types of instability can be classified according to the dominant terms in Eq. 14:

- *Magnetic-Damping-Controlled Instability (single-mode flutter):* The dominant terms are associated with the symmetric damping matrix $[C_1]$. Flutter arises because the magnetic damping forces create "negative damping," that is, a magnetic force that acts in phase with the vehicle velocity.

- *Magnetic-Stiffness-Controlled Instability (coupled-mode flutter):* The dominant terms are associated with the antisymmetric stiffness matrix $[K_2]$. It is called coupled-mode flutter because at least two modes are required to produce it.

Corresponding to the single- and coupled-mode flutter, parametric and combination resonances may exist if the motion-dependent magnetic forces are a periodic function of time.

- *Parametric Resonance:* When the period of a motion-dependent magnetic force is a multiple of one of the natural frequencies of the vehicle, the vehicle may be dynamically unstable.

- *Combination Resonance:* When the period of the motion-dependent magnetic forces is equal to the sum or difference divided by an ﹍integer of the natural frequencies of the vehicle, the vehicle may also be subjected to dynamic instability.

In practical cases, two or more mechanisms may interact with one another, and Eq. 12 is applicable for general cases.

It is noted that maglev systems are subjected to several groups of forces, including magnetic forces, aerodynamic forces, and guideway perturbation. The theory presented in this paper is applicable to maglev systems when they are subjected to other types of forces. In particular, the aerodynamic effects can be described exactly the same way as those given in Eqs. 1-14 and the dynamic response characteristics to aerodynamic forces are similar to magnetic forces; see Chen (1987) for details.

4   Simplified Vehicle Models for Dynamic Instability

Four different vehicles are considered, in order to provide an understanding of stability characteristics.

4.1 Two-Degree-of-Freedom Vehicle

A maglev vehicle is supported by magnetic forces; the resultant lift and drag forces of the coil above the continuous-sheet track can be represented approximately by (Sinha 1987)

$$F_L(v,z,t) = \varepsilon_L F(t),$$

$$F_D(v,z,t) = \varepsilon_D F(t),$$

$$F(t) = \mu_0 I^2/4\pi z,$$

$$\varepsilon_L = 1 - 1/(1 + v^2/w^2)^n,$$

$$\varepsilon_D = (w/v)[1 - 1/(1 + v^2/w^2)^n],$$

$$w = 2/\mu_0 \sigma h,$$

(15)

where v is the forward velocity, z is the steady-state height of the coil above the track, t is the time, I is the constant coil current, and w is the characteristic speed and is related to track thickness h, conductivity σ, and permeability μ_0. The value of n is 1 for a single conductor and varies from about 1/5 to 1/3 for coils (Rhodes and Mulhall 1981). Note that $F(t)$ represents the repulsive force between the coil and its image coil. The force ratios, ε_L and ε_D, are given in Fig. 6 for $n = 1$, 1/3, and 1/5.

Assume that the vehicle is traveling at a velocity v_0 at an equilibrium height z_0. The instantaneous position and height of the vehicle are x and z respectively; therefore,

$$x(t) = v_0 t + X(t),$$

$$z(t) = z_0 + Z(t).$$

(16)

The equations of motion for the vehicle moving at a velocity $v(t)$ with a levitation height $z(t)$ can be written as

$$m\ddot{z}(t) = -mg + F_L(v,z,t),$$

$$m\ddot{x}(t) = F_p - F_D(v,z,t) - F_a,$$

(17)

where m is the mass of the vehicle, F_p is the propulsion force, and F_a is the aerodynamic force. The aerodynamic force is given by
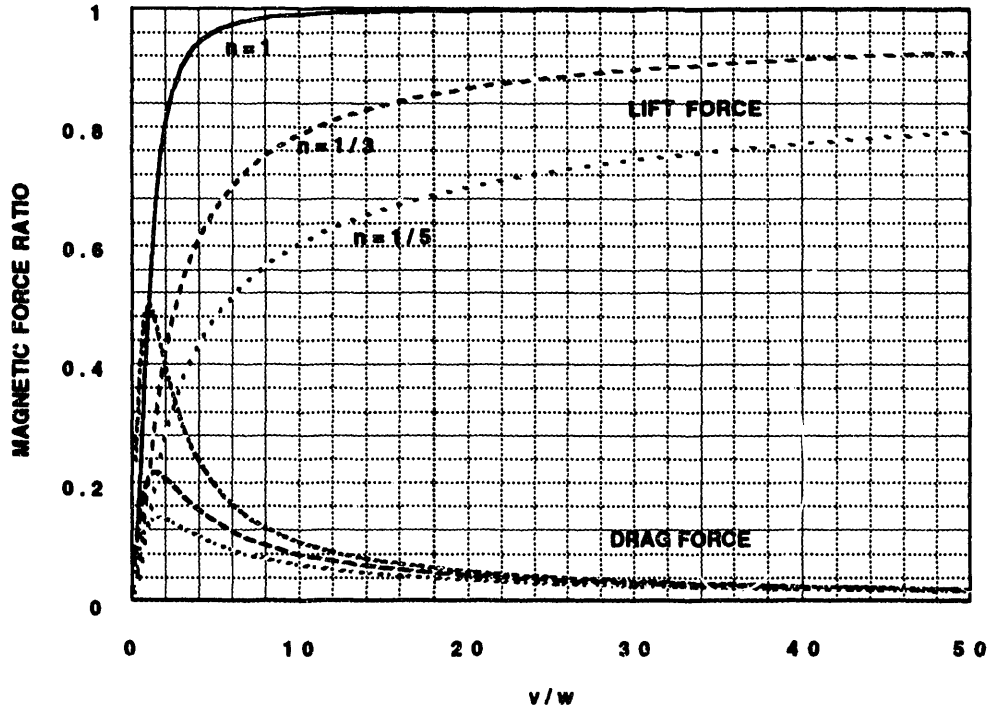
Fig. 6. Magnetic forces divided by image force

$$F_a = K_a v^2,$$

$$K_a = 0.5\ C_D LA\rho,$$

(18)

where L and A are the length and cross-sectional area of the vehicle, ρ is air density, C_D is the drag coefficient (with its values varying from 0.2 to 0.3, depending on vehicle shape).

The equilibrium point of the vehicle v_0 and z_0 is defined by

$$F_L(v_0,z_0) = mg,$$

$$F_D(v_0,z_0) = F_p - F_a.$$

(19)

Using Eqs. 16-19 and neglecting the nonlinear terms, we obtain the following equations of motion for the vehicle X(t) and Z(t):

$$m\ddot{Z}(t) - C_{zx}(v,z,t)\dot{X}(t) + K_{zz}(v,z,t)Z(t) = 0,$$

$$m\ddot{X}(t) + C_{xx}(v,z,t)\dot{X}(t) - K_{xz}(v,z,t)Z(t) = 0.$$

(20)

$C_{zx}(v,z,t)$ and $C_{xx}(v,z,t)$ are magnetic damping, and $K_{zz}(v,z,t)$ and $K_{xz}(v,z,t)$ are magnetic stiffness; these are given by

$$C_{zx}(v,z,t) = \partial F_L(v,z,t)/\partial v \mid_{(v_0,z_0)},$$

$$C_{xx}(v,z,t) = \partial F_D(v,z,t)/\partial v \mid_{(v_0,z_0)} + 2K_a v_0,$$

$$K_{zz}(v,z,t) = -\partial F_L(v,z,t)/\partial z \mid_{(v_0,z_0)}, \tag{21}$$

$$K_{xz}(v,z,t) = -\partial F_D(v,z,t)/\partial z \mid_{(v_0,z_0)}.$$

Their values are given as follows:

$$C_{zx} = (mg/\varepsilon_L)2nv_0/[w^2(1 + v_0^2/w^2)^{n+1}],$$

$$C_{xx} = wmg/v_0^2 [w^2 - (2n - 1)v_0^2/(w^2 + v_0^2)] + 2K_a v_0,$$

$$K_{zz} = mg/z_0, \tag{22}$$

$$K_{xz} = wmg/v_0 z_0.$$

For high speed vehicles, the values of C_{zx} and K_{xz} are approximately zero. Therefore, the motions in the vertical direction and forward direction are uncoupled at high speeds.

Equations 20 can be analyzed; let

$$Z(t) = a \exp(i\omega t),$$

$$X(t) = b \exp(i\omega t). \tag{23}$$

Substituting Eqs. 23 into Eqs. 20 gives the following frequency equation:

$$\begin{bmatrix} -m\omega^2 + K_{zz} & -i\omega C_{zx} \\ -K_{xz} & -m\omega^2 + i\omega C_{xx} \end{bmatrix} \begin{Bmatrix} a \\ b \end{Bmatrix} = \begin{Bmatrix} 0 \\ 0 \end{Bmatrix}. \tag{24}$$

The natural frequencies can be determined from the determinant of the coefficient matrix given in Eq. 24. At high speeds, the off-diagonal terms may be neglected. The natural frequency of the vertical motion f_v is

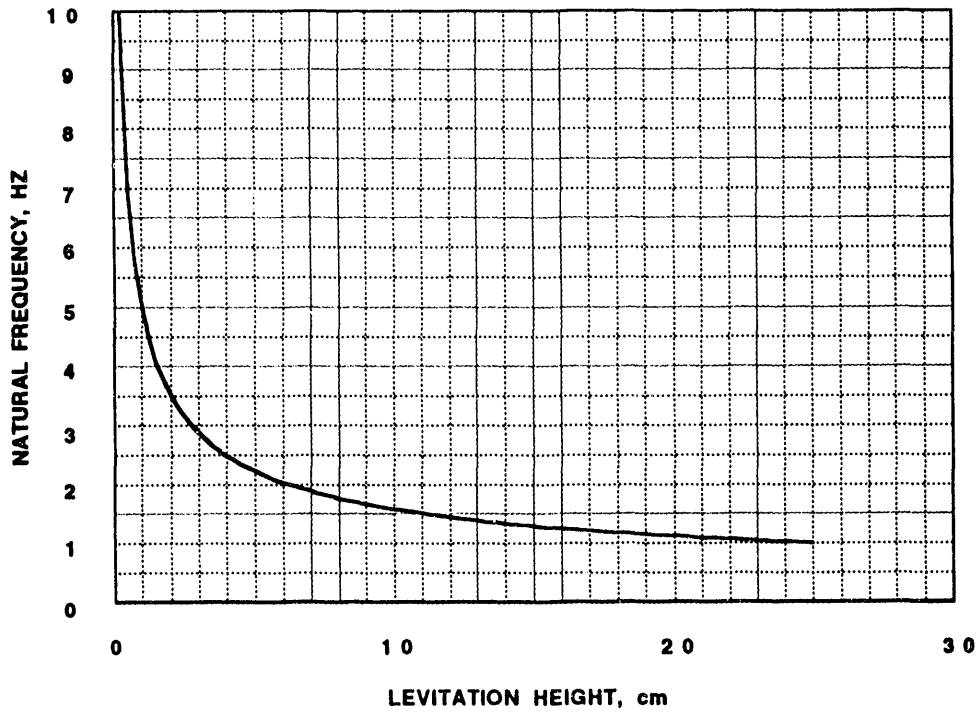$$f_v = (g/z_0)^{0.5}/2\pi. \tag{25}$$

Fig. 7. Natural frequency as a function of levitation height

The natural frequency in the vertical direction depends on the levitation height only. Figure 7 shows the natural frequency as a function of the levitation height. At high speeds, oscillations in the vertical direction are stable.

In the forward direction, the motion is given by

$$X(t) = C_1 + C_2 \exp(st). \tag{26}$$

For high-speed vehicles, the exponent s is approximately given by

$$s = (2n - 1)wg/v_0^2 - 2K_a v_0. \tag{27}$$

Note that the vehicle may be unstable if $n = 1$, and K_a is zero. At high speeds, the second term given in Eq. 27 is larger than the first term regardless of the values of n; therefore, s is negative and the system is stable.

4.2 Three-Degree-of-Freedom Vehicle

Figure 8 shows a three-degree-of-freedom vehicle traveling at a velocity v_0 at an equilibrium height z_0. For a symmetric vehicle, the instantaneous position and height of the vehicle are $x(t)$, $z_1(t)$, and $z_2(t)$; therefore,
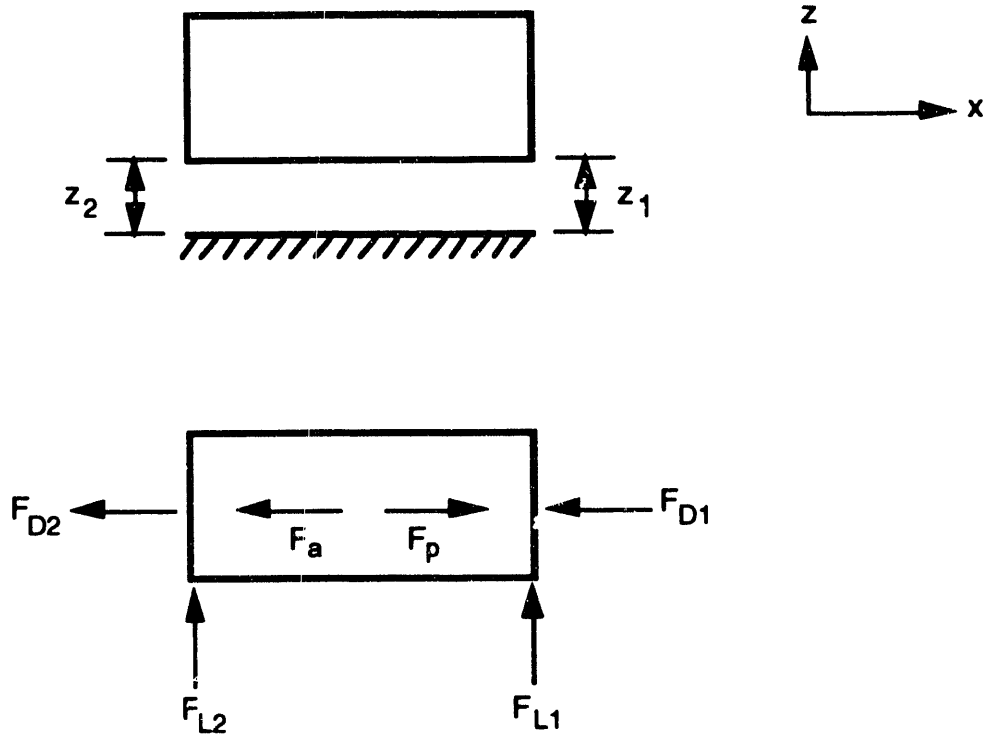
Fig. 8. Three-degree-of-freedom vehicle

$$x(t) = v_0(t) + X(t) \,,$$

$$z_1(t) = z_0 + Z_1(t) \,, \tag{28}$$

$$z_2(t) = z_0 + Z_2(t) \,.$$

The equations of motion for the vehicle moving at a velocity $v(t)$ with levitation height $z_1(t)$ and $z_2(t)$ can be written as

$$m\ddot{x}(t) = F_p - F_{D1}(z_1,v,t) - F_{D2}(z_2,v,t) - F_a,$$

$$\frac{m}{2}\left[\ddot{z}_1(t) + \ddot{z}_2(t)\right] = -mg + F_{L1}(z_1,v,t) + F_{L2}(z_2,v,t), \tag{29}$$

$$\frac{I_\theta}{L}\left[\ddot{z}_1(t) - \ddot{z}_2(t)\right] = \frac{L}{2}\left[F_{L1}(z_1,v,t) - F_{L2}(z_2,v,t)\right].$$

where m is the vehicle mass, I_θ is the rotational moment of inertia about the vehicle's center of mass, F_p is the propulsion force, and F_a is the aerodynamic force that is assumed to act at the center of mass of the vehicle and is given by Eq. 18.

For a symmetric vehicle with two identical levitation systems at the two ends, the equilibrium point of the vehicle v_0, z_{10}, and z_{20}, as well as the magnetic forces, is defined as

$$F_{L1}(v_0, z_{10}) + F_{L2}(v_0, z_{20}) = mg \; ,$$

$$F_{D1}(v_0, z_{10}) + F_{D2}(v_0, z_{20}) = F_p - F_a \; ,$$

$$z_{10} = z_{20} = z_0 \; , \tag{30}$$

$$F_{L1}(v_0, z_{10}) = F_{L2}(v_0, z_{20}) \; ,$$

$$F_{D1}(v_0, z_{20}) = F_{D2}(v_0, z_{20}) \; .$$

Using Eqs. 28, 29, 30, and 18 and neglecting the nonlinear terms, we obtain the following equations of motion of the vehicle, $X(t)$, $Z_1(t)$, and $Z_2(t)$:

$$\frac{m}{2}(\ddot{Z}_1 + \ddot{Z}_2) + (C_{zx1} + C_{zx2})\dot{X} + K_{zz1}Z_1 + K_{zz2}Z_2 = 0$$

$$\frac{2I_\theta}{L^2}(\ddot{z}_1 - \ddot{z}_2) + (C_{zx1} - C_{zx2})\dot{X} + (K_{zz1}Z_1 - K_{zz2}Z_2 = 0 \tag{31}$$

$$m\ddot{X} + (C_{xx1} + C_{xx2} + 2k_a v_0)\dot{X} + K_{xz1}Z_1 + K_{xz2}Z_2 = 0$$

where

$$C_{zxi} = -\frac{\partial F_{Li}}{\partial v}\bigg|_{(v_0, z_0)}$$

$$C_{xxi} = \frac{\partial F_{Di}}{\partial v}\bigg|_{(v_0, z_0)}$$

$$\tag{32}$$

$$K_{zzi} = -\frac{\partial F_{Li}}{\partial z_i}\bigg|_{(v_0, z_0)}$$

$$K_{xzi} = \frac{\partial F_{Di}}{\partial z_i}\bigg|_{(v_0, z_0)}$$

$$i = 1, 2.$$

The magnetic damping coefficients C_{zxi} and C_{xxi}, and the magnetic stiffness coefficients K_{zzi} and K_{xzi} can be calculated from the magnetic lift and drag forces given in Eq. 15.

At high speeds, K_{zxi} and C_{xzi} are approximately zero. The equations of motion become

$$\frac{m}{2}(\ddot{Z}_1 + \ddot{Z}_2) + K_{zz1}Z_1 + K_{zz2}Z_2 = 0,$$

$$\frac{2I_\theta}{L^2}(\ddot{Z}_1 - \ddot{Z}_2) + K_{zz1}Z_1 - K_{zz2}Z_2 = 0, \tag{33}$$

$$m\ddot{X} + (C_{xx1} + C_{xx2} + 2K_a v_0)\dot{X} = 0.$$

In this case, the vehicle is stable at high speeds; this is similar to the two-degree-of-freedom vehicle. The natural frequency of vertical oscillations is the same as that in the two-degree-of-freedom system given in Eq. 25. The natural frequency of pitching oscillations is

$$f_p = \frac{1}{2\pi}\left(\frac{L^2 mg}{4I_\theta z_0}\right)^{0.5}. \tag{34}$$

For a square vehicle with length L and height h, the natural frequency of pitching oscillations is

$$f_p = \frac{1}{2\pi}\left(\frac{g}{z_0}\right)^{0.5}\left(\frac{3}{1+\frac{h^2}{L^2}}\right)^{0.5}. \tag{35}$$

The natural frequency of pitching oscillations is larger than vertical oscillations. For a long vehicle (h << L), f_p is equal to about 1.7 f_v. For a square vehicle, f_p = 1.4 f_v. At high speeds, heaving and pitching oscillations are stable for the magnetic levitation described by Eq. 15. In the forward direction, the result is the same as that for the two-degree-of-freedom vehicle.

4.3 Six-Degree-of-Freedom Vehicle

For the six-degree-of-freedom vehicle shown in Fig. 1, stability can be studied from Eqs. 11 or 12. Once the coefficients of magnetic forces m_{ij}, c_{ij}, and k_{ij} are known, Eqs. 11 or 12 can be evaluated for $Q = 0$. Let the displacement of a particular component be

$$u_j(t) = a_j \exp(\lambda + i\omega)t .$$ (36)

Substituting Eq. 36 into Eq. 12 with $Q = 0$ yields

$$\left\{ (\lambda + i\omega)^2[M] + (\lambda + i\omega)[C] + [K] \right\} \{A\} = \{0\} .$$ (37)

The values of λ and ω can be calculated based on Eq. 37 by setting the determinant of the coefficient matrix equal to zero.

Vehicle stability is determined by λ, which is a function of v. If $\lambda < 0$, vehicle motion is damped; if $\lambda > 0$, vehicle displacement increases with time until nonlinear effects become important.

To solve this problem, all motion-dependent magnetic-force coefficients must be known. At this time, it appears that limited analytical, numerical, or experimental data are available. For any future maglev systems, it will be necessary to investigate the characteristics of motion-dependent magnetic forces to avoid dynamic instabilities.

4.4 Vehicle on Double L-Shaped Aluminum Sheet Guideway

Figure 9 shows a cross section of a vehicle on a double L-shaped aluminum sheet guideway. Assume that the vehicle travels at a constant velocity along x direction. Two permanent magnets are attached to the bottom of vehicle and provide lift and guidance force F_{L_1}, F_{L_2}, F_{G_1}, and F_{G_2} (see Fig. 9). Assume at the initial state that $h_1 = h_2 = h_0$ and $g_1 = g_2 = g_0$; thus, the vehicle and guideway geometries can be expressed as follows:

$$L_1 = L_2 = S = 76.2 \ (mm)$$
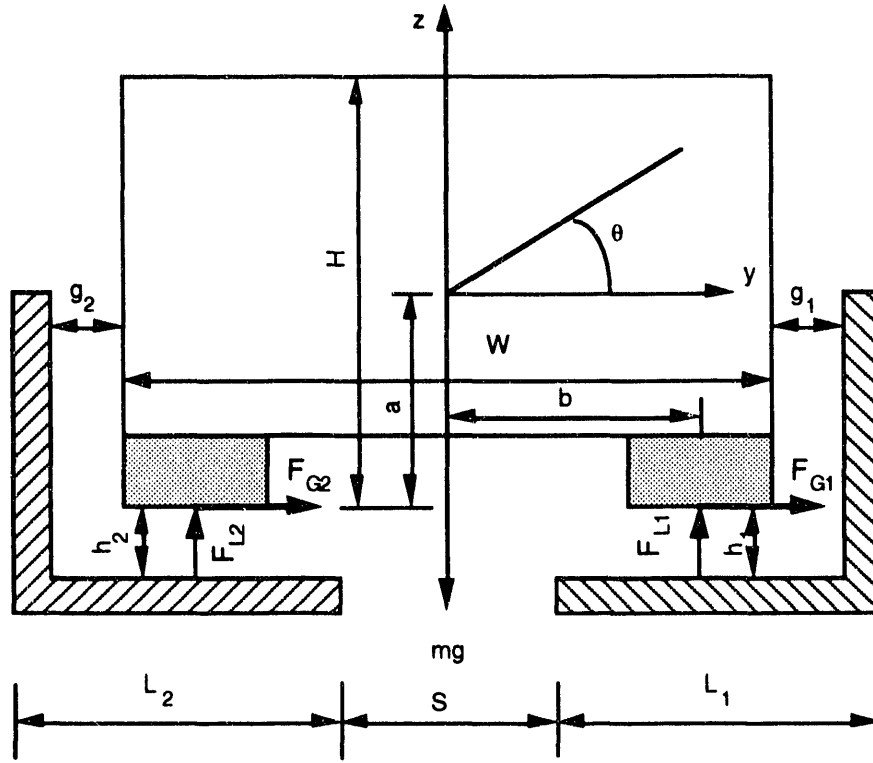
$$W = 152.4 + S - 2g_0 \ (mm)$$

$$H = 0.9 \ W \ (mm)$$

Fig. 9. Maglev system with a vehicle operating on double L-shaped aluminum sheet guideway

$a = 0.5\, H$ (mm)

$b = 0.5(W - 25.4)$ (mm).

Equations of motion for this three-degree-of-freedom maglev system can be written as

$$m\ddot{z} + C\dot{z} = F_{L_1} + F_{L_2} - mg$$

$$I\ddot{\theta} + E\dot{\theta} = \left(F_{G_1} + F_{G_2}\right)a + \left(F_{G_1} + F_{G_2}\right)b \qquad (38)$$

$$m\ddot{y} + D\dot{y} = F_{G_1} + F_{G_2},$$

where m is the mass of the vehicle, C and D are damping ratios; I is the moment of inertia about the center of mass inertia moment of the vehicle [I = $(m/12)(H^2 + W^2)$]. F_{L_1}, F_{L_2}, F_{G_1}, and F_{G_2} are lift and guidance forces and are functions of y and z. At the equilibrium position, they are $F_{L_{10}}(y_0,z_0)$, $F_{L_{20}}(y_0,z_0)$, $F_{G_{10}}(y_0,z_0)$, and $F_{G_{20}}(y_0,z_0)$. Apply them to Eqs. 38:

$$F_{L10} = F_{L20}$$

$$F_{L10} + F_{L20} = mg \tag{39}$$

$$F_{G10} = -F_{G20}$$

Therefore

$$m = \frac{F_{L10} + F_{L20}}{g} = \frac{2F_L(h_o)}{g}. \tag{40}$$

Let

$$\left. \begin{aligned} z &= \frac{1}{2}(u_1 + u_2) \\ y &= u_3 \\ \theta &= (u_1 - u_2)/2b \end{aligned} \right\}, \tag{41}$$

where u_1, u_2, and u_3 are shown in Fig. 10. Equations 38 can be rewritten as

$$m(\ddot{u}_1 + \ddot{u}_2) + c(\dot{u}_1 - \dot{u}_2) = 2\left(F_{L_1} + F_{L_2} - mg\right)$$

$$\frac{I}{b}(\ddot{u}_1 - \ddot{u}_2) + \frac{E}{b}(\dot{u}_1 - \dot{u}_2) = 2a\left(F_{G_1} + F_{G_2}\right) + 2b\left(F_{G_1} - F_{G_2}\right) \tag{42}$$

$$m\ddot{u}_3 + D\dot{u}_3 = F_{G_1} + F_{G_2}.$$

Note the reduced dependence of the forces on the new displacements of Eq. 41:

$$F_{L_1} = F_{L_1}(u_1, u_3)$$

$$F_{L_2} = F_{L_2}(u_2, u_3)$$

$$\tag{43}$$

$$F_{G_1} = F_{G_1}(u_1, u_3)$$
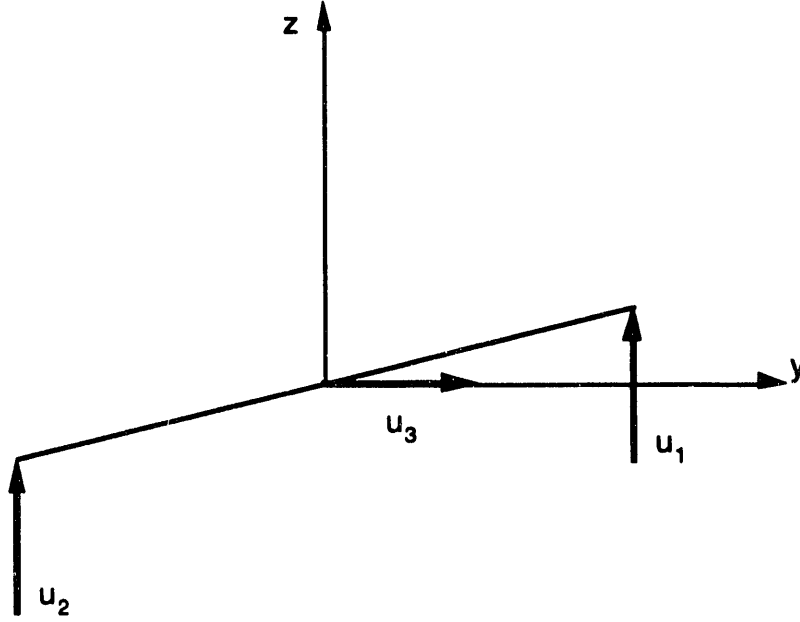
$$F_{G_2} = F_{G_2}(u_2, u_3).$$

Fig. 10. **Displacement components of three-degree-of-freedom vehicle**

Let

$$u_i = u_{io} + v_i \qquad i = 1, 2 \tag{44}$$

The linear approximation of lift and guidance forces can be expressed as

$$F_{L_1} = F_{L_{10}} + \frac{\partial F_{L1}}{\partial v_1} v_1 + \frac{\partial F_{L1}}{\partial v_3} v_3$$

$$F_{L_2} = F_{L_{20}} + \frac{\partial F_{L2}}{\partial v_2} v_2 + \frac{\partial F_{L2}}{\partial v_3} v_3$$

$$\tag{45}$$

$$F_{G_1} = F_{G_{10}} + \frac{\partial F_{G1}}{\partial v_1} v_1 + \frac{\partial F_{G1}}{\partial v_3} v_3$$

$$F_{G_2} = F_{G_{20}} + \frac{\partial F_{G2}}{\partial v_2} v_2 + \frac{\partial F_{G2}}{\partial v_3} v_3$$

Using Eqs. 39 and 45, we can rewrite Eq. 42 as

$$\ddot{v}_1 + \ddot{v}_2 + \frac{C}{m}\dot{v}_1 + \frac{C}{m}\dot{v}_2 - \frac{2}{m}\frac{\partial F_{L_1}}{\partial v_1}v_1 - \frac{2}{m}\frac{\partial F_{L_2}}{\partial v_2}v_2 - \frac{1}{m}\left(\frac{\partial F_{G_1}}{\partial v_3} + \frac{\partial F_{G_2}}{\partial v_3}\right)v_3 = 0$$

$$-\ddot{v}_1 + \ddot{v}_2 - \frac{E}{I}\dot{v}_1 + \frac{E}{I}\dot{v}_2 + \left(\frac{2cb}{I}\frac{\partial F_{L_1}}{\partial v_1} + \frac{2b^2}{I}\frac{\partial F_{G_1}}{\partial v_1}\right)v_1$$

$$+\left(\frac{2ab}{I}\frac{\partial F_{L_2}}{\partial v_2} + \frac{2b^2}{I}\frac{\partial F_{G_2}}{\partial v_2}\right)v_2 \qquad (46)$$

$$+\left[\frac{2ab}{I}\left(\frac{\partial F_{L_1}}{\partial v_3} + \frac{\partial F_{L_2}}{\partial v_3}\right) + \frac{2b^2}{I}\left(\frac{\partial F_{G_1}}{\partial v_3} + \frac{\partial F_{G_2}}{\partial v_3}\right)\right]v_3 = 0$$

$$\ddot{v}_3 + \frac{D}{m}\dot{v}_3 - \frac{1}{m}\frac{\partial F_{L_1}}{\partial v_1}v_1 - \frac{1}{m}\frac{\partial F_{L_2}}{\partial v_2}v_2 - \frac{1}{m}\left(\frac{\partial F_{L_1}}{\partial v_3} + \frac{\partial F_{L_2}}{\partial v_3}\right)v_3 = 0$$

or

$$[M]\{\ddot{v}\} + [C]\{\dot{v}\} + [K]\{v\} = 0 \qquad (47)$$

where

$$M = \begin{bmatrix} 1 & 1 & 0 \\ -1 & 1 & 0 \\ 0 & 0 & 1 \end{bmatrix}, \qquad C = \begin{bmatrix} c_{11} & c_{22} & 0 \\ c_{21} & c_{22} & 0 \\ 0 & 0 & c_{23} \end{bmatrix}, \qquad K = \begin{bmatrix} k_{11} & k_{12} & k_{13} \\ k_{21} & k_{22} & k_{23} \\ k_{31} & k_{32} & k_{33} \end{bmatrix}, \qquad (48)$$

and

$$c_{11} = c_{12} = \frac{C}{m}$$

$$c_{21} = -c_{22} = -\frac{E}{I}$$

$$c_{33} = \frac{D}{m}$$

$$k_{11} = -\frac{2}{m}\frac{\partial F_{L_1}}{\partial v_1} \qquad (49)$$

$$k_{12} = -\frac{2}{m}\frac{\partial F_{L_2}}{\partial v_2}$$

$$k_{13} = -\frac{1}{m}\left(\frac{\partial F_{L_1}}{\partial v_3} + \frac{\partial F_{L_2}}{\partial v_3}\right)$$

$$k_{21} = \frac{2ab}{I}\frac{\partial F_{G_1}}{\partial v_1} + \frac{2b^2}{I}\frac{\partial F_{L_1}}{\partial v_1}$$

$$k_{22} = \frac{2ab}{I}\frac{\partial F_{G_2}}{\partial v_2} - \frac{2b^2}{I}\frac{\partial F_{L_2}}{\partial v_2}$$

$$k_{23} = \frac{2ab}{I}\left(\frac{\partial F_{G_1}}{\partial v_3} + \frac{\partial F_{G_2}}{\partial v_3}\right) + \frac{2b^2}{I}\left(\frac{\partial F_{L_1}}{\partial v_3} + \frac{\partial F_{L_2}}{\partial v_3}\right)$$

(49)
(Cont'd)

$$k_{31} = -\frac{1}{m}\frac{\partial F_{G_1}}{\partial v_1}$$

$$k_{32} = -\frac{1}{m}\frac{\partial F_{G_2}}{\partial v_2}$$

$$k_{33} = -\frac{1}{m}\left(\frac{\partial F_{G_1}}{\partial v_3} + \frac{\partial F_{G_2}}{\partial v_3}\right)$$

where

$$\frac{\partial F_{L_1}}{\partial v_1} = k_{\ell\ell}(h), \qquad \frac{\partial F_{G_1}}{\partial v_1} = -k_{g\ell}(h),$$

$$\frac{\partial F_{L_2}}{\partial v_2} = k_{\ell\ell}(h), \qquad \frac{\partial F_{G_2}}{\partial v_2} = k_{g\ell}(h),$$

(50)

$$\frac{\partial F_{L_1}}{\partial v_3} = k_{\ell g}(g), \qquad \frac{\partial F_{G_1}}{\partial v_3} = k_{gg}(g),$$

$$\frac{\partial F_{L_2}}{\partial v_3} = k_{\ell g}(g), \qquad \frac{\partial F_{G_2}}{\partial v_3} = k_{gg}(g).$$

$k_{\ell\ell}(h)$, $k_{\ell g}(g)$, $k_{g\ell}(h)$, and $k_{gg}(g)$ are motion-dependent magnetic-force coefficients (see Fig. 5).

If we assume that the damping effects can be neglected, the eigenvalues of Eq. 47 can be obtained from

$$[K]\{v\} = \lambda [M]\{v\} \tag{51}$$

where $\lambda = \omega_R + i\,\omega_I$.

With magnetic forces and stiffnesses measured by the experiments (see Figs. 4 and 5), the eigenvalues and eigenvectors of a maglev vehicle on a double L-shaped guideway were calculated with the theoretical model developed in this section. Some very interesting results were obtained from those calculations.

Figure 11 shows that eigenvalues of vehicle motion versus levitation height vary when guidance gaps are fixed ($g_1 = g_2 = Y^* = 12.7$ mm). The first mode ω_1 shows an uncoupled heave motion; its imaginary part of the eigenvalue is zero, while the second and third modes are coupled roll-sway motions. Within the range of height $h = 19.0$ to 35 mm, the imaginary parts of the eigenvalues appear not to be zero. This indicates that within this range, flutter does exist for these coupled roll-sway vibrations. Table 1 and Fig. 12 give eigenvectors and modal shapes of these three modes of vehicle motion, respectively. When the guidance gaps are fixed at $g_1 = g_2 = Y^* = 5$ mm, the same results are obtained, as shown in Fig. 13; there is a flutter for coupled roll-sway modes.

Table 1. Eigenvectors of vehicle motion ($Y^* = 12.7$ mm)

Mode	h = 15.0 mm			h = 25 mm			h = 37 mm		
	v_1	v_2	v_3	v_1	v_2	v_3	v_1	v_2	v_3
Uncoupled heave mode ω_1	1	1	0	1	1	0	1	1	0
Coupled roll-sway mode ω_2	1	−1	−0.009	0.586	−0.586	−0.332	−1	1	−0.205
Coupled roll-sway mode ω_3	−0.545	0.545	1	−0.810	0.810	0.060	1	−1	0.448
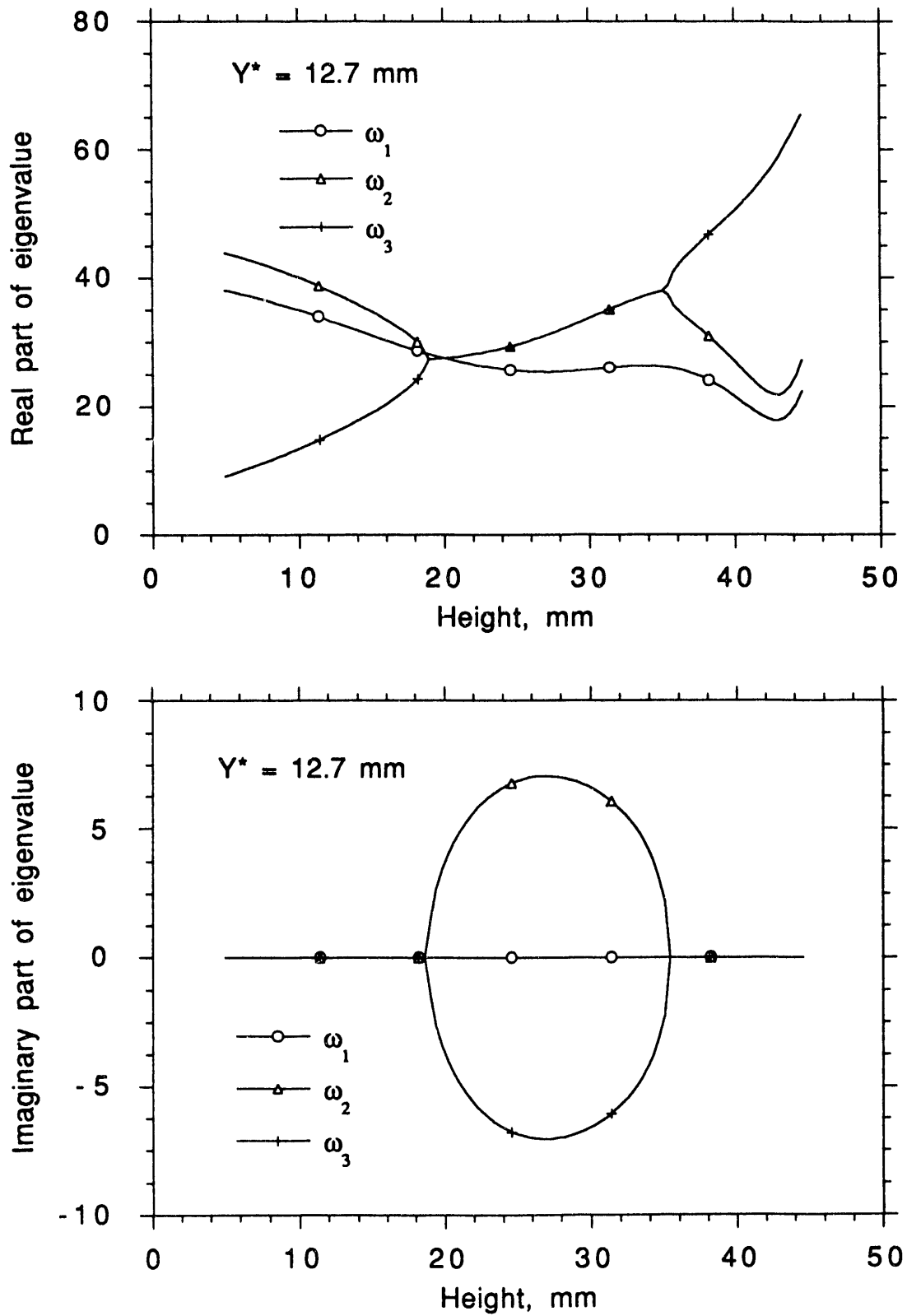
Fig. 11. Maglev-system eigenvalues vs. vehicle levitation height, with Y* = 12.7 mm

Uncoupled Heave Mode ω_1

Coupled Roll-Sway Mode ω_2

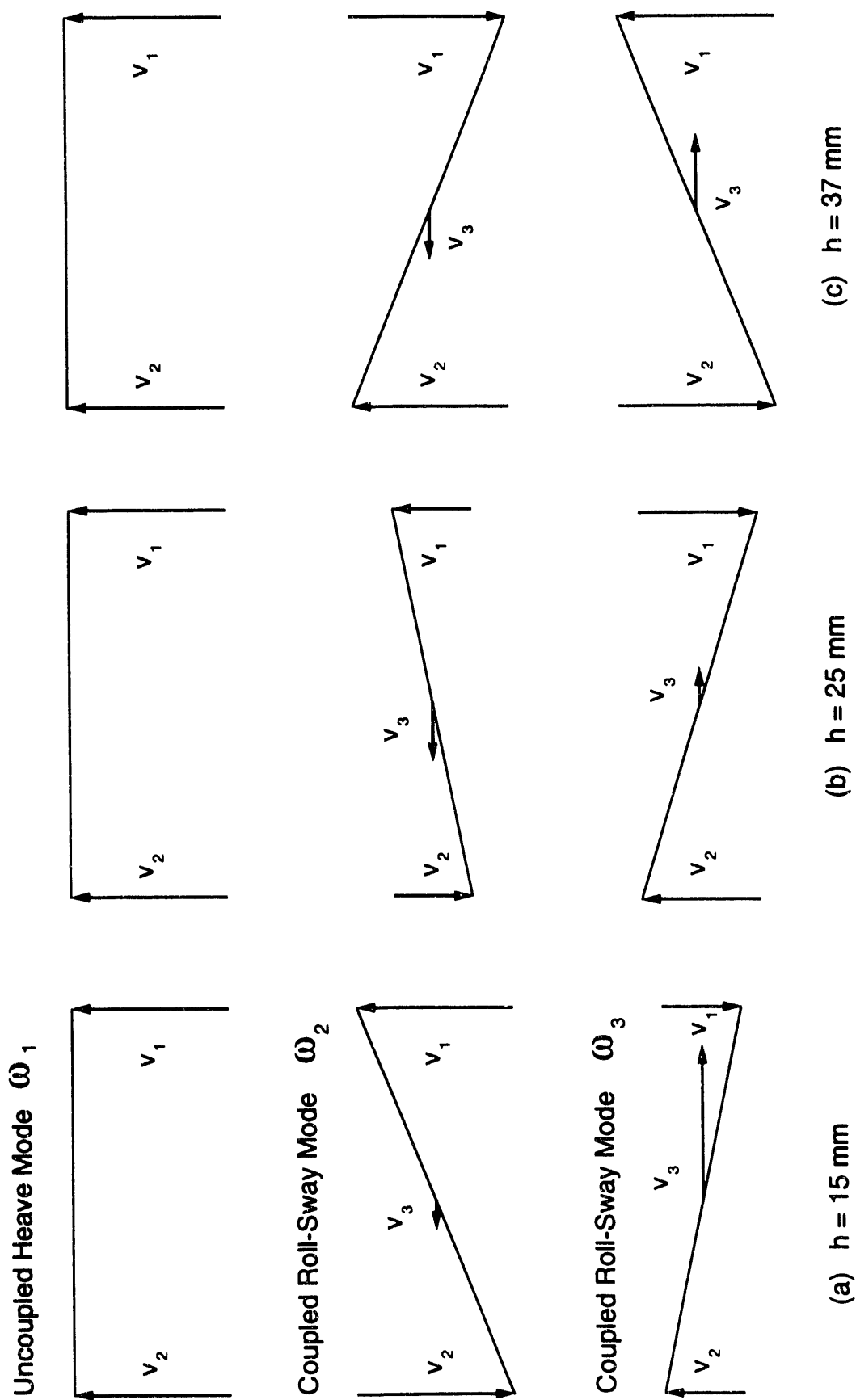Coupled Roll-Sway Mode ω_3

(a) h = 15 mm

(b) h = 25 mm

(c) h = 37 mm

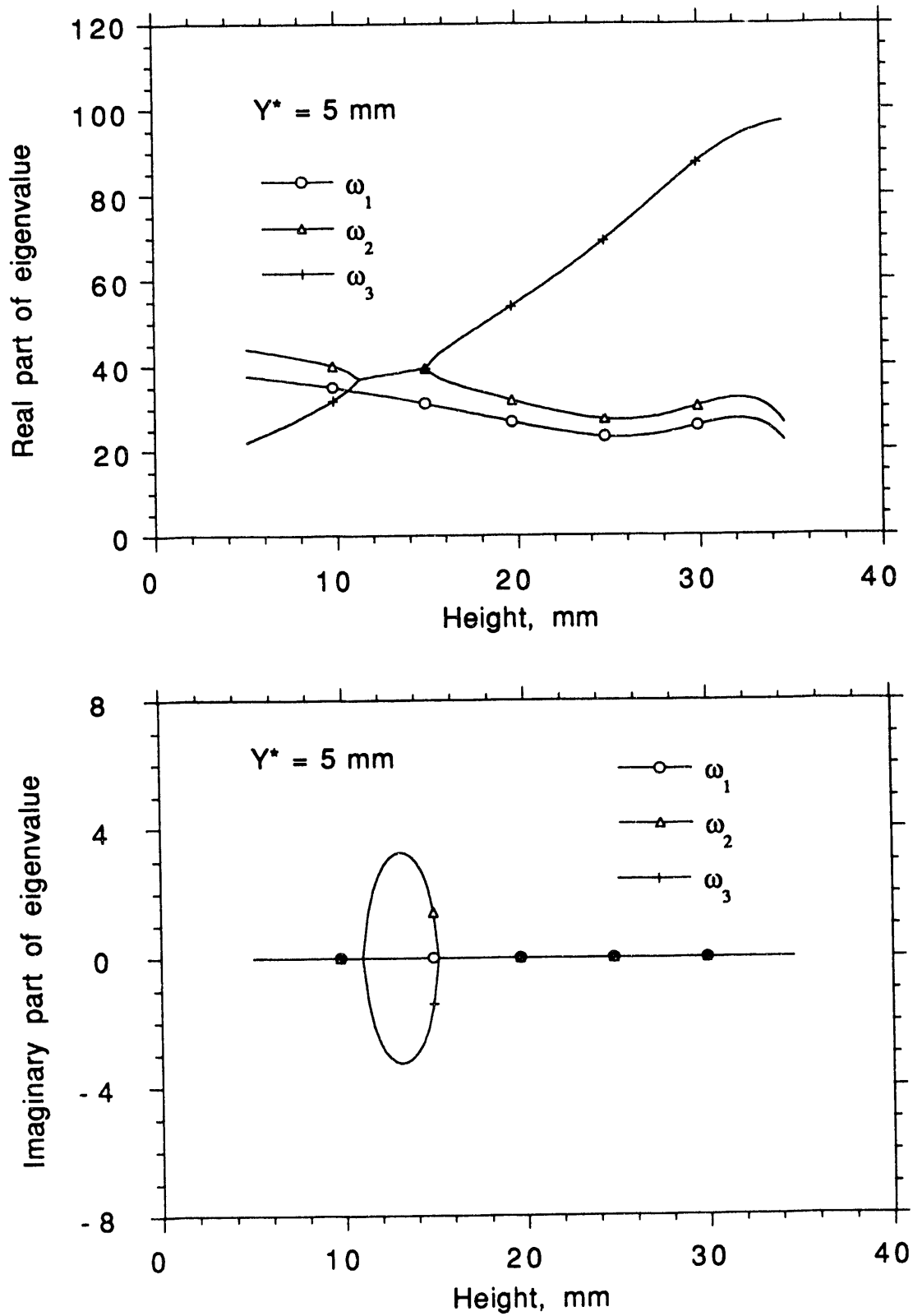*Fig. 12. Modal shapes of three-degree-of-freedom maglev system with $Y^* = 12.7$ mm*

Fig. 13. *Maglev-system eigenvalues vs. vehicle levitation height,*
with Y* = 5 mm

Figures 14 and 15 show eigenvalues of vehicle motion versus lateral location of vehicle when $g_1 = g_2 = g_0 = 25$ mm and levitation heights $h = 12.7$ mm and $h = 7$ mm, respectively. We notice that for the third mode, which presents the transversal motion of vehicle, the real part is zero and imaginary part is not zero within a certain region. This indicates that the divergence is subjected to the lateral motion of the vehicle, given those vehicle and guideway parameters. Figure 16 shows the real part of the third mode versus lateral location of vehicle when the parameter-equilibrium guidance gap varies as $g_1 = g_2 = g_0 = 10$ mm, 15 mm, 20 mm, and 25 mm. We found that divergence appears only in the case of $g_0 = 25$ mm.

We must point out that the measured and calculated data for motion-dependent magnetic-forces and force coefficients are very limited and that damping effects were not considered in the above analysis. Even though divergence and flutter appear in the eigenvalue results, we still have difficulty in completely predicting the dynamic instability of this three-degree-of-freedom maglev vehicle model. Further research is needed in modeling to gain an understanding of dynamic instability in maglev systems.

5   Closing Remarks

- Motion-dependent magnetic forces are the key elements in modeling and understanding dynamic instabilities of maglev systems. At this time, it appears that very limited data are available for motion-dependent magnetic forces. Efforts will be made to compile analytical results and experimental data for motion-dependent magnetic forces. When this work is completed, recommendations will be presented on research needs on magnetic forces. In addition, specific methods to obtain motion-dependent magnetic forces will be described in detail.

- Various options can be used to stabilize a maglev system: passive electrodynamic primary suspension damping, active electrodynamic primary suspension damping, passive mechanical secondary suspension, and active mechanical secondary suspension. With a better understanding of vehicle stability characteristics, a better control law can be adopted to ensure a high level of ride comfort and safety.
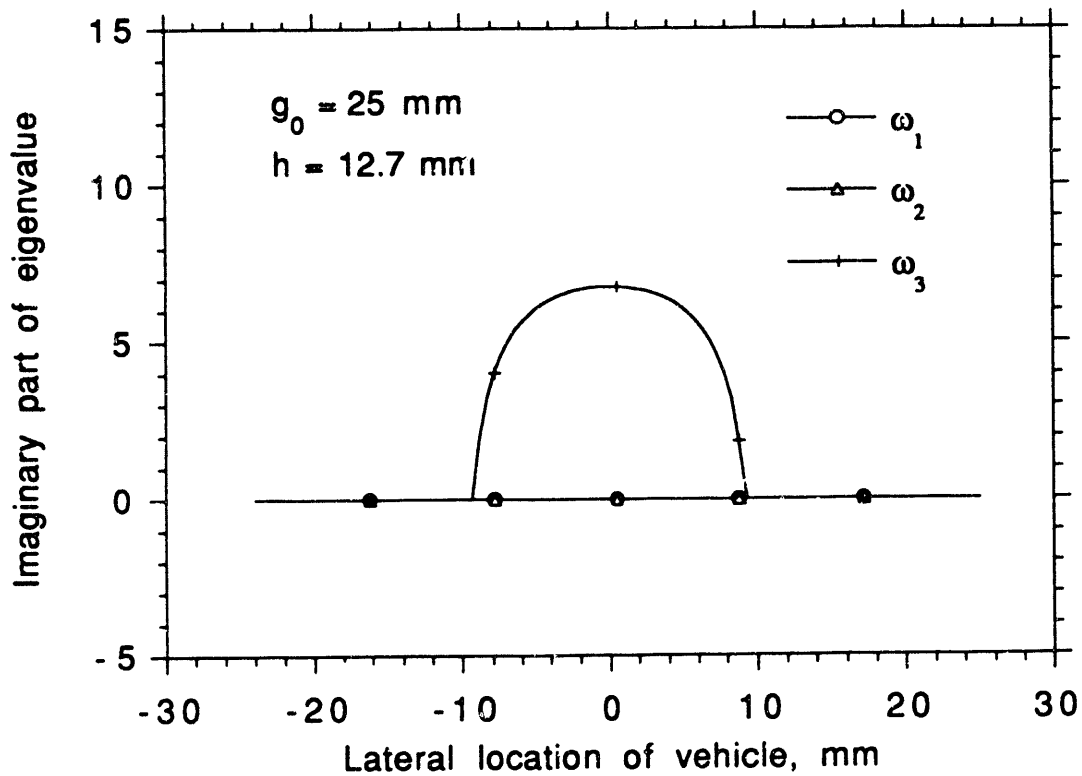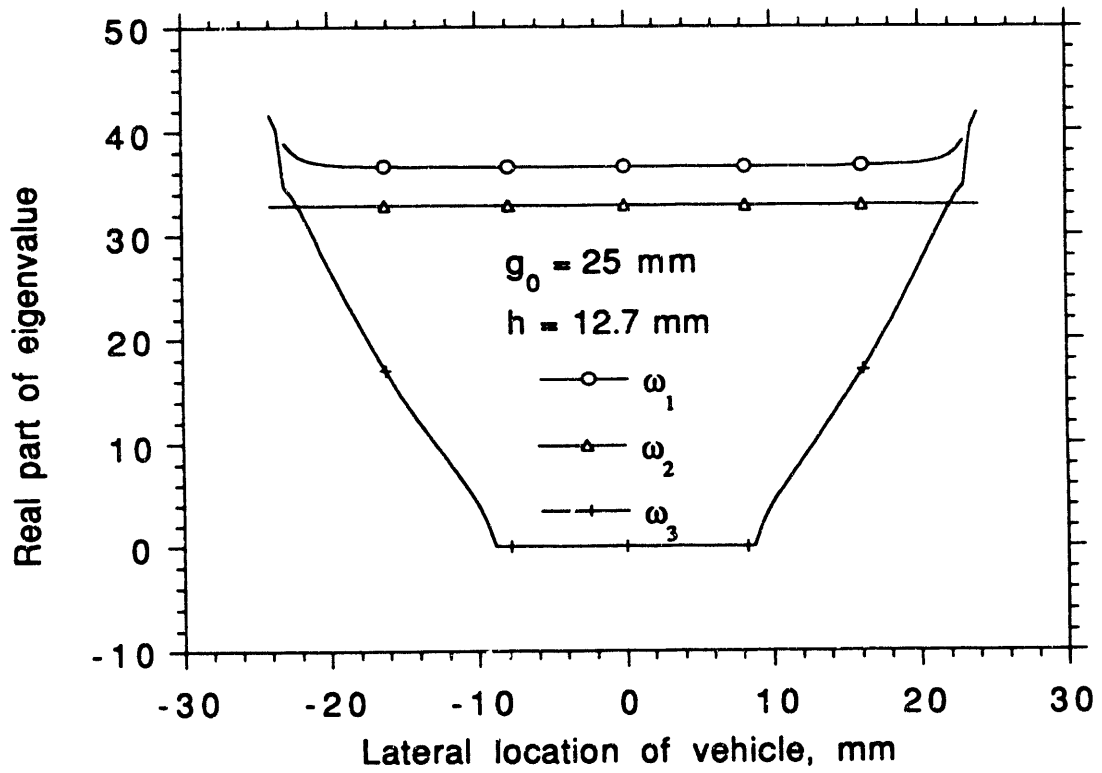
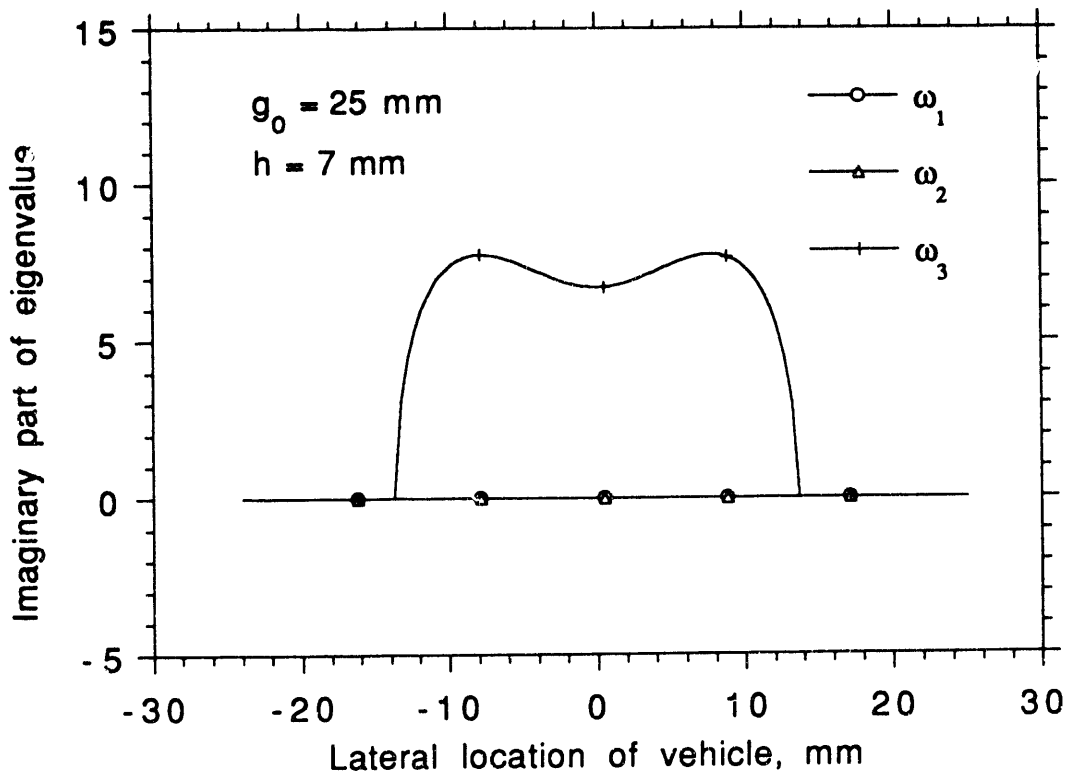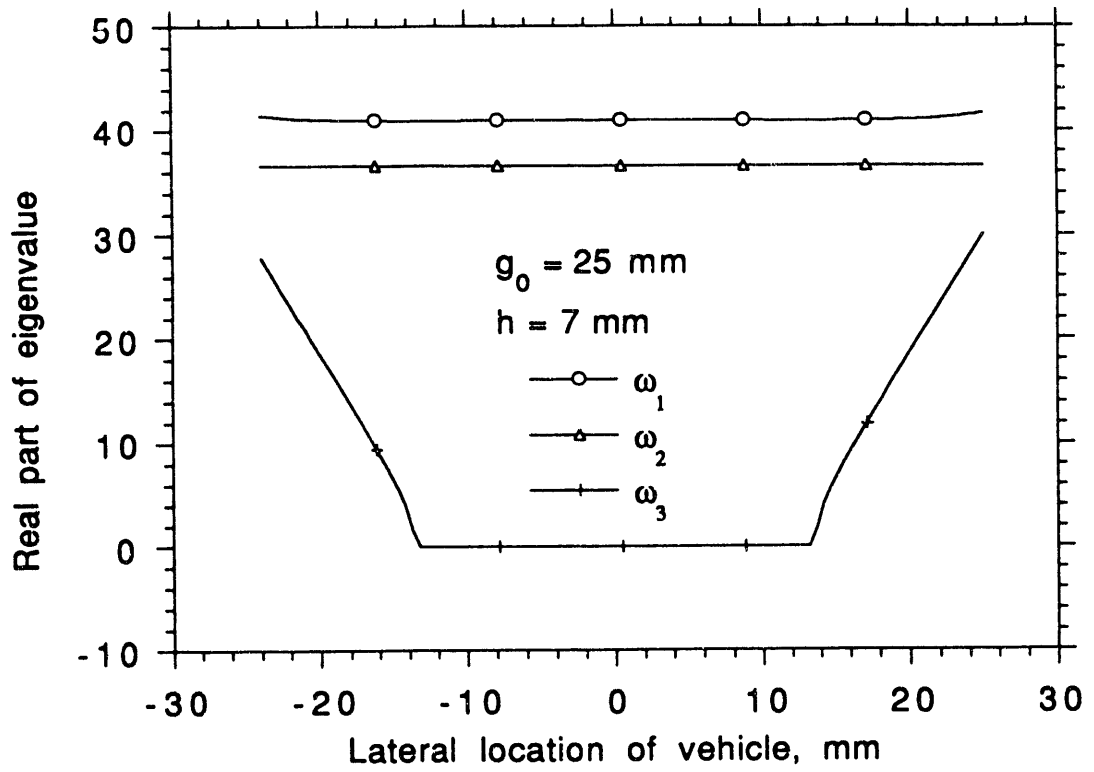*Fig. 14. Maglev-system eigenvalues vs. lateral location of vehicle, with h = 12.7 mm and g_0 = 25 mm*

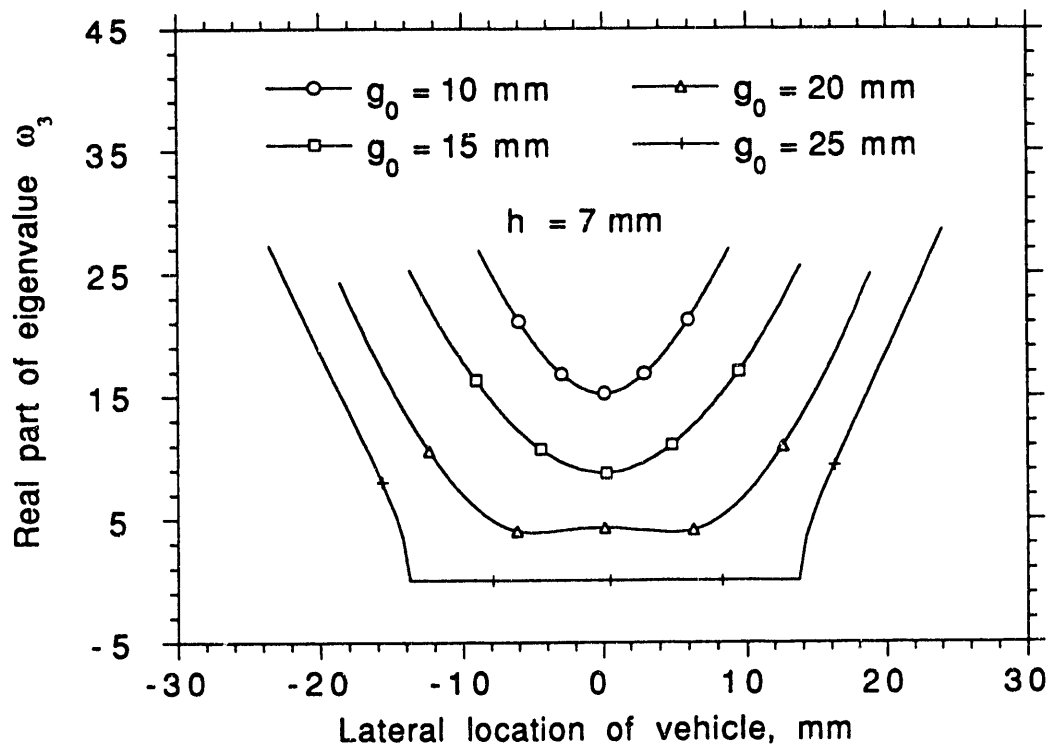Fig. 15. Maglev-system eigenvalues vs. lateral location of vehicle, with h = 7 mm and g_0 = 25 mm

Fig. 16. Real part of maglev-system eigenvalues vs. lateral location of vehicle, with h = 7 mm and g_0 = 10, 15, 20, and 25 mm

- Computer programs are needed to screen new system concepts, evaluate various designs, and predict vehicle response. It appears that the stability characteristics of maglev vehicles under different conditions have not been studied in detail in existing computer codes. When information on motion-dependent magnetic forces becomes available, the existing computer codes can be significantly improved.

- Instabilities of maglev-system models have been observed at Argonne and other organizations. An integrated experimental/analytical study of stability characteristics is an important aspect of maglev research.

Acknowledgments

References

Chen, S. S. (1987), *Flow-Induced Vibration of Circular Cylindrical Structures*, Hemisphere Publishing Co., New York.

Chu, D., and Moon, F. C. (1983), *Dynamic Instabilities in Magnetically Levitated Models*, J. Appl. Phys. **54**(3), pp. 1619-1625.

Davis, L. C., and Wilkie, D. F. (1971), *Analysis of Motion of Magnetic Levitation Systems: Implications*, J. Appl. Phys. **42**(12), pp. 4779-4793.

Moon, F. C. (1974), *Laboratory Studies of Magnetic Levitation in the Thin Track Limit*, IEEE Trans. on Magnetics, MAG-10, No. 3, pp. 439-442 (September 1974).

Moon, F. C. (1975), "Vibration Problems in Magnetic Levitation and Propulsion," *Transport Without Wheels*, ed. by E. R. Laithwaite, Elek Science, London, pp. 122-161.

Ohno, E., Iwamoto, M., and Yamada, T. (1973), *Characteristic of Superconductive Magnetic Suspension and Propulsion for High-Speed Trains*, Proc. IEEE **61**(5), pp. 579-586.

Rhodes, R. G., and Mulhall, B. E. (1981), *Magnetic Levitation for Rail Transport*, Oxford University Press, New York.

Sinha, P. K. (1987), *Electromagnetic Suspension, Dynamics and Control*, Peter Peregrinus Ltd, London, United Kingdom.

Yabuno, H., Takabayashi, Y., Yoshizawa, M., and Tsujioka, Y. (1989), *Bounding and Pitching Oscillations of a Magnetically Levitated Vehicle Caused by Guideway Roughness*, Int. Conference Maglev 89, pp. 405-410.

Distribution for ANL–92/21

Internal

Y. Cai (10)
S. S. Chen (10)
J. L. He
L. R. Johnson
C. A. Malefyt (2)
T. M. Mulcahy (5)
D. M. Rote (5)
R. A. Valentin

M. W. Wambsganss (3)
Z. Wang
R. W. Weeks
S. Zhu
ANL Patent Dept.
ANL Contract File
TIS Files (3)

External

DOE–OSTI for distribution per UC–330 (91)
ANL–TIS Libraries (2)
Manager, Chicago Operations Office, DOE
Director, Technology Management Div., DOE–CH
D. L. Bray, DOE–CH
A. L. Taboas, DOE–CH
Materials and Components Technology Division Review Committee:
    H. K. Birnbaum, University of Illinois at Urbana-Champaign, Urbana
    R. C. Buchanan, University of Illinois at Urbana-Champaign, Urbana
    M. S. Dresselhaus, Massachusetts Institute of Technology, Cambridge, MA
    B. G. Jones, University of Illinois at Urbana-Champaign, Urbana
    C.-Y. Li, Cornell University, Ithaca, NY
    S.-N. Liu, Electric Power Research Institute, Palo Alto, CA
    R. E. Smith, Engineering Applied Sciences, Inc., Trafford, PA
O. P. Manley, DOE, Washington, DC
J. S. Coleman, DOE, Washington, DC
D. Frederick, DOE, Washington, DC
F. C. Moon, Cornell University, Ithaca, NY

END

DATE
FILMED

2 / 19 / 93